COMMUNICATIONS OF THE GEOLOGICAL SURVEY OF NAMIBIA

VOLUME 25
2022

MINISTRY OF MINES AND ENERGY

MINISTRY OF MINES AND ENERGY

Deputy Permanent Secretary Geological Survey: Gloria Simubali

COMMUNICATIONS OF THE GEOLOGICAL SURVEY OF NAMIBIA

VOLUME 25
2022

Referees : H. Mocke, U.M Schreiber, M. Pickford

Manuscript handling : U.M. Schreiber, M. Pickford, K. Mhopjeni

Obtainable from the Geological Survey
Private Bag 13297, Windhoek, Namibia

ISSN 1026-2954

COMMUNICATIONS OF THE GEOLOGICAL SURVEY OF NAMIBIA

VOLUME 25
2022

CONTENTS

Cover Image

Panoramic view of Teufelskuppe : a carbonatite occurrence in the Northern Sperrgebiet, Namibia, viewed from the southwest

(Photo M. Pickford, 2018)

The Keishöhe carbonatites of southwestern Namibia – the post-magmatic role of silicate xenoliths on REE mobilisation

Benjamin F. Walter[1,2] , Johannes Giebel[3,4], Alan G. Marlow[5], Pete R. Siegfried[6], Michael Marks[7], Gregor Markl[7], Martin Palmer[8], Jochen Kolb[1]

[1] *Karlsruhe Institute of Technology (KIT), Institute for Applied Geosciences, Chair of Economic Geology and Geochemistry, Adenauerring 20b, 76131 Karlsruhe, Germany (b.walter@kit.edu)*
[2] *Laboratories of Environmental and Raw Material Analyses (LERA), Adenauerring 20b, 76131 Karlsruhe*
[3] *Technische Universität Berlin, Ernst-Reuter-Platz 1, 10587 Berlin, Germany*
[4] *University of the Free State, 250 Nelson-Mandela-Drive, Bloemfontein 9300, South Africa*
[5] *Avanti Resources, Mornington, Victoria, 3931, Australia*
[6] *Camborne School of Mines, University of Exeter, Cornwall, UK*
[7] *University of Tübingen, GUZ, Schnarrenbergstraße 94 & 96, Tübingen, Germany*
[8] *University of Southampton, School of Ocean and Earth Science, University of Southampton, Southampton SO14 3ZH, UK*

Abstract :- Exploration for rare earth element (REE)-deposits hosted in carbonatites and associated rocks is challenging because of the heterogeneous distribution of REE and the variable and often complex mineralogy of such REE mineralisation. The Keishöhe in southwestern Namibia is a subvolcanic intrusion consisting of calcite-carbonatite, dolomite-carbonatite, ankerite-carbonatite dykes, ring dykes and diatremes, and is regarded to be a part of the Kudu lineament carbonatite complexes.

Importantly, it exemplifies many of the problems associated with REE exploration – particularly regarding its heterogeneous REE distribution. It is therefore an excellent site in which to explore the processes related to REE precipitation in detail. Petrography, whole rock geochemistry and microXRF imaging of xenolith-bearing and xenolith-free carbonatites provide insight into the role of silicate xenoliths in the development of a hydrothermal or supergene REE mineralisation in a subvolcanic environment. Xenolith-rich carbonatites are almost barren, whereas xenolith-free carbonatites show REE-contents of up to 10 wt. % total REE (TREE). Therefore, the probability for REE-enrichment in the various Keishöhe carbonatites is significantly higher in the absence of silicate rock xenoliths. The REE mineralisation is dominated by REE-F-carbonates, while monazite is a minor constituent. In contrast to other complexes, where Si assimilation caused REE depletion in the melt during the magmatic stage, this study demonstrates post-magmatic hydrothermal or supergene REE mobilisation and enrichment. REE remobilisation and enrichment is caused by hydrothermal or supergene alteration of silicate xenoliths (Si release) by aqueous fluid(s). In combination with previous studies this study clearly shows that silicate xenoliths have 1) a significant influence on REE-mineralisation in general and 2) may act either positively (precipitation/incorporation) or negatively (mobilisation) on the mineralisation of discrete REE phases depending upon the related syn-magmatic or post-magmatic processes.

Key Words :- Carbonatite, Ring dykes, Rare Earth Elements, MicroXRF, Sperrgebiet, Tsau-ǁKhaeb-(Sperrgebiet)-National Park, southern Namib, Mineralisation, Xenoliths

To cite this paper :- Walter, B.F., Giebel., R.J, Marlow, A.G., Siegfried, P.R., Marks, M., Markl, G., Palmer, M. & Kolb, J. 2022. The Keishöhe carbonatites of southwestern Namibia – the post-magmatic role of silicate xenoliths on REE mobilisation. *Communications of the Geological Survey of Namibia*, **25**, 1-31.

Introduction

Carbonatites are defined as igneous rocks that consist predominantly of carbonate minerals (e.g. calcite, dolomite, ankerite) and minor phosphates, oxides and silicates (Le Maitre *et al*. 2002; Yaxley *et al*. 2022). About 600 carbonatite occurrences are currently known worldwide, with the majority (~80%) being associated with a diverse suite of alkaline silicate rocks (Mitchell, 2005; Humphreys-Williams & Zahirovic, 2021). Most carbonatite

occurrences formed in a continental rift setting or lie along crustal-scale lineaments (Woolley & Kjarsgaard, 2008). Carbonatites are classified by their dominant carbonate phase into calcite-, dolomite-, natro- and ankerite-carbonatites (Woolley & Kempe, 1989). Calcite-carbonatites are most common, whereas large-scale, primary magmatic dolomite-ankerite carbonatites are much less abundant. However, the latter may frequently be emplaced as late dykes and ring dykes that commonly crosscut the major calcite-carbonatite. To explain the origin of carbonatite melts two petrogenetic models are considered. Firstly, direct formation as low-degree partial mantle melts (Bell & Simonetti, 2010; Dalton & Presnall, 1998; Moore & Wood, 1998), and secondly from a carbonate-bearing silicate melt by fractional crystallization (Lee & Wyllie, 1994) and/or liquid-liquid immiscibility (Veksler *et al*. 1998).

During ascent to crustal levels, the magmatic evolution is furthermore driven by processes such as (a) immiscibility between carbonate, oxide, fluoride and sulphide melts; (b) crystal fractionation; (c) interaction with and assimilation of diverse wall rocks; and (d) multi-stage release of aqueous-carbonic fluids of variable salinity resulting in wall-rock autometasomatism (e.g. Elliot *et al*. 2018; Giebel *et al*. 2019a, b; Walter *et al.* 2020, 2021; Berkesi *et al*. 2020).

Carbonatites host mineral deposits of mainly REE, Nb, P, Fe, Zr and fluorite (Mariano, 1989; Goodenough *et al*. 2018; Anenburg *et al*. 2021, and references therein), and 50-60 carbonatites are currently being mined. Examples are Mountain Pass (USA), Palabora (South Africa), Okorusu (Namibia), Bayan Obo (China), Mount Weld (Australia), St. Honoré (Canada) and Kovdor (Russia) (Castor, 2008; Gendron *et al*. 1984; Giebel *et al*. 2017; Ivanyuk *et al*. 2016; Lottermoser, 1990; Smith *et al*. 2015). Intense exploration and mine development is currently underway at Kangankunde, Tundulu, Songwe Hill (all in Malawi) and Fen (Finland) (Broom-Fendley *et al*. 2017; Chikanda *et al*. 2019; Dietzel *et al*. 2019). More than 40% of REE exploration projects worldwide target carbonatites (Chakhmouradian & Wall, 2012; Chakhmouradian & Zaitsev, 2012; Kynicky *et al*. 2012). Nevertheless, exploitation for carbonatite-hosted REE deposits is challenging and costly due to their complex mineralogy, geometry and heterogeneity, which typically results in complex process engineering and high plant capital costs. Furthermore, all these aspects play an important role in determining the economic value of carbonatite-hosted REE deposits (Edahbi *et al*. 2018). In most of the mined deposits enhanced REE enrichment and REE mineral formation is attributed to late-magmatic stages. Consequently, it is often assumed that highly evolved carbonatites (i.e., dolomite-carbonatites, ankerite-carbonatites) are better-endowed in REE (Wall & Mariano, 1996). Recent field-based and experimental studies have also shown that carbonatite–wall rock interaction may affect the development of economic grade REE mineralisation in both early and late stages of the intrusion (Anenburg *et al*. 2020; Giebel *et al*. 2019b).

The Keishöhe carbonatite is located in the Tsau-ǁKhaeb-(Sperrgebiet)-National Park, in southwestern Namibia and is an ideal site to study the effect of crustal contamination on REE mineralisation in carbonatites, because highly mineralised and poorly mineralised dolomite-carbonatite dykes occur together, and silicate rock xenoliths are abundant. Furthermore, within the same structural part of the complex, the weakly mineralised lithologies are rich in siliceous crustal xenoliths. This contribution provides the first detailed description of the Keishöhe carbonatite and demonstrates the potential impact of xenolith contamination under hydrothermal/supergene conditions on the REE mineralisation of a carbonatite.

Geological Setting

The Keishöhe carbonatite is located in the access-restricted, and hence poorly studied, Tsau-ǁKhaeb-(Sperrgebiet)-National Park in SW Namibia (Fig. 1). Access to the area has been restricted for more than a hundred years to protect the diamond mining operations along the coast. To date, three alkaline magmatic events are known in the area between Lüderitz and Aus in Namibia and Keishöhe likely belongs to the youngest: (1) Intrusive alkaline magmatic activity occurred during the ~1.1 Ga Namaqua Orogeny (Walter *et al.*, in prep.). So far, only the deformed Glockenberg carbonatite is known from this orogen in Namibia (Walter *et al*. in prep.) which is located about 20 km northwest of Keishöhe; (2) Mainly intrusive

alkaline magmatism formed the ~130 Ma Lüderitz Alkaline Province including several larger syenite intrusions near the Sperrgebiet coast south of Lüderitz (Granitberg, Pomona and Drachenberg) and numerous unnamed minor syenite plugs and dykes (Marsh, 1973, 1975a, 1975b, 1976; Reid *et al*. 1990); (3) The youngest alkaline and carbonatitic magmatic event (~45-50 Ma, age constraints are only available for Dicker Willem and the Klinghardt Mountains) is either related to the formation of volcanic nephelinitic rocks, Dreyer Rücken and Swartkop close to the Klinghardt Mountains (Kaiser, 1926; Stocken, 1978) and the Tsirub nephelinites close to Aus and close to Keishöhe (Nakashole *et al*. 2020), or to volcanic phonolites of the Klinghardt Mountains and the subvolcanic Dicker Willem carbonatite (Kröner, 1973; Lock & Marsh, 1981; Marsh, 1987; Marsh, *et al*. 2018; Reid *et al*. 1990). Five carbonatite bodies, namely Dicker Willem (also known as Garub Berg, Dikwillem), Keishöhe (Keishöhe), Teufelskuppe (also known as Twyfelskupje, Zweifelskuppe, Trufelkuppe, Kalup), Kaukausib, Chameis (Panther) and Karingarab, are hosted by the large-scale Kudu lineament or conjugate structures (Corner, 2000; Marlow & Palmer, in press). The complexes hosted by the Kudu lineament are therefore summarised as Kudu lineament carbonatite complexes.

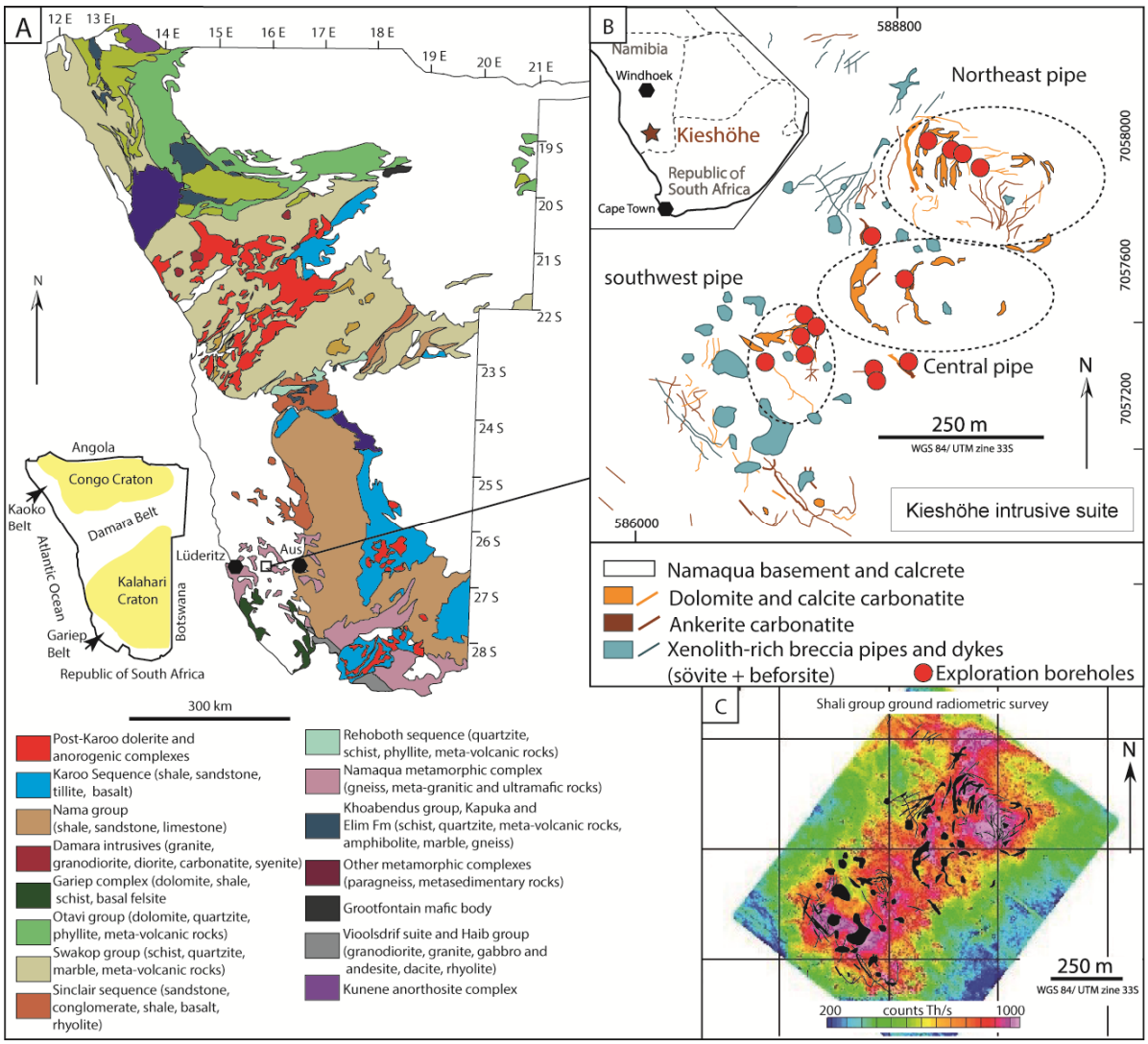

Figure 1. A) Simplified geological map of Namibia (modified from Miller 2008). B) Geological map of the Keishöhe carbonatite complex (Shilongo, 2014). C) Ground radiometric map (Shilongo, 2014). Thorium response on all carbonatites is high compared to the wall rocks. Black signature depicts the various carbonatite outcrops. Note: The geometry of the ring dykes when interpreted as related to caldera or maar formation indicates a shallow and subvolcanic erosion level.

The other alkaline igneous complexes southwest of Keishöhe include Granitberg, Drachenberg, Pomona/Signalberg and minor nephelinites and melilitites. They all show evidence for a deeper emplacement level (Marsh, 1975a, 1975b). However, their genetic relation to the Kudu lineament carbonatites is unclear, since only Dicker Willem (49 Ma) is dated (being assumed to be representative for the Kudu lineament) and only a single 133 Ma age for Granitberg (Reid *et al*. 1990) indicates an earlier phase of igneous activity.

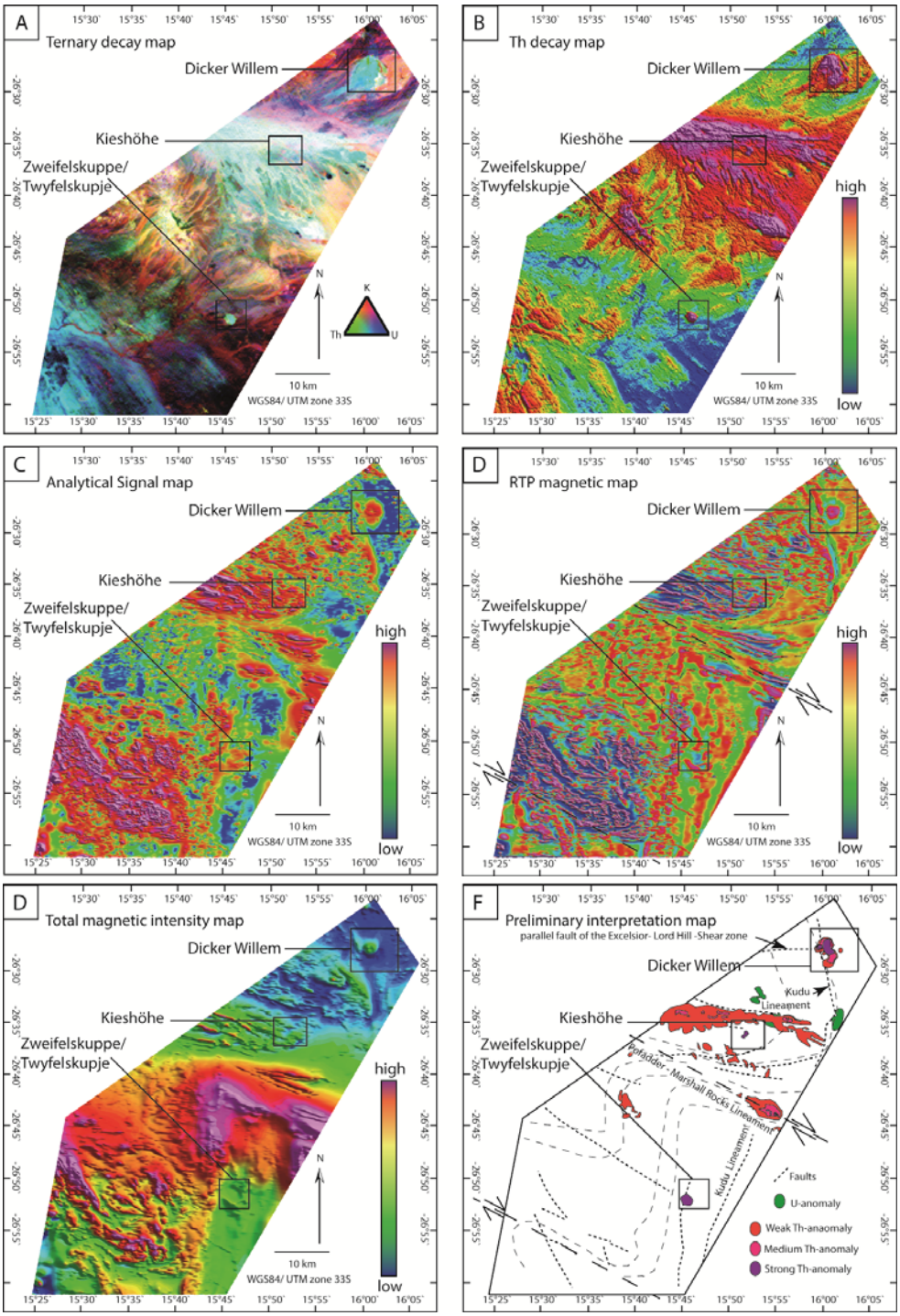

Figure 2. Regional scale government airborne geophysical data purchased and provided by the Shali Group. A) Ternary plot of K, Th and U decays. B) Th decay map. C) Analytical signal map. D) Reduced to pole (RTP) map. E) Total magnetic intensity map. F) Preliminary geophysical interpretation. Note: Carbonatite complexes of Dicker Willem, Keishöhe and Teufelskuppe (Twyfelskupje) are each situated at the intersection of two main lineaments (NNW-NNE striking Kudu Lineament and NW-SE structures of the Namaqua Metamorphic Complex).

The Keishöhe Carbonatite Complex

The Keishöhe carbonatite forms a series of low hills about ~7 km southeast of the old Keishöhe railroad siding (Fig. 1B, 2). It intruded gneiss, quartzite and schist of the Meso-proterozoic Namaqua Metamorphic Complex (Jackson, 1976; Cooper, 1988). It is spatially associated with the Dicker Willem and Teufelskuppe carbonatites situated on the NNE-SSW striking Kudu lineament and its parallel faults (Fig. 2).

The Keishöhe carbonatite consists of sills and ring dykes in a NE-SW striking outcrop measuring 1.3 km in length and 900 m in width. It is defined by scattered outcrops and Th channel ground radiometric mapping (Fig. 1C). The carbonatites form three individual outcrops of stacked, shallow dipping ring dykes and associated dykes, with the majority having a common thickness of 1-7 metres. At least three different ring systems are distinguished, referred to as the Northeast, Central and Southwest pipes (Fig. 1). The Northeast pipe is the best exposed and consists of an asymmetric stack of ring dykes and associated dykes, with the inferred long axis plunging steeply to the northwest (Fig. 3A-E). Individual ring dykes are typically between 2 and 5 metres thick, and are separated by a few to tens of metres of poorly exposed, weathered and oxidised basement rocks. Some of the ring dykes contain silicate rock xenoliths from the wall rocks. They are up to 1 m across. A 2 m wide carbonatite rich in xenoliths forms the outermost dyke on the northern edge of the Northeast pipe (Fig. 3F).

The Central pipe consists of two, up to about 5 m thick, ring dykes that are separated by basement rocks which dip towards the east. The Southwest pipe consists of more densely spaced and thinner stacked ring dykes. They are surrounded by 5 to 20 metre (diameter) thick carbonatite breccia pipes and breccia dykes, as well as brecciated quartzite and silicified rocks (Fig. 3G).

Layering in the ring dykes is typically shallow to moderately dipping (Fig. 3D, E). Rare flow banding dips steeply with a northern inclination. Two major types of carbonatites are distinguished: A) Dolomite-carbonatite and B) ankerite-carbonatite. Dolomite-carbonatite is dominantly brown, with subordinate yellow ankerite-carbonatite (Fig. 3D, E). Transitions between yellow ankerite-carbonatite and brown dolomite-carbonatite are common. Calcite-carbonatites are rare and strongly altered.

The ring dykes are crosscut by narrow (1-2 m thick) dolomite-carbonatite dykes and breccia diatremes with fragments of gneiss, schist, syenite, alkali granite, quartzite and amphibolite which are part of the Namaqua Metamorphic Complex. Some of the breccia diatremes are situated at the intersection of two dykes, which may belong to either ring dykes or crosscutting dykes.

Dolomite-carbonatites contain lenses of secondary “iron ore” with alunite as a further dominant mineral. Minor fine-grained phonolite veins with porphyritic K-feldspars are only observed in drill core. They are fenitised and crosscut by dolomite-carbonatite of both dyke systems. In the direct vicinity (several metres) of the dykes, gneiss, quartzite, amphibolite, schist and marble of the Namaqua Metamorphic Complex show hydrothermal and/or supergene alteration.

Sample material

Fifty samples were taken from outcrops exposed in trenches and from 14 diamond drill holes (tested depth between 59.5 m and 215.3 m) recovered during an exploration program by the Shali Group in 2017/18 which transect the entire regolith profile. Weathering at Keishöhe is deep, and fresh carbonatite was reached in only two boreholes at a depth of about 50 metres (Fig. 4, 5). The upper two metres of outcrops showed intensive weathering, including Liesegang rings (Fig. 6A), and is underlain by a deep zone of intermediate weathering and saprolite formation that extends to a depth of ~50 metres, as evidenced from drill core). Fresh examples of late-stage calcite-carbonatite veins are only rarely observed in the drill cores below the supergene alteration zone, and associated alkaline silicate rocks are represented only by minor phonolite veins observed from the bottom of the 215 m drill hole (hole ID J111-001). These phonolite veins are similar to those observed in the vicinity of Dicker Willem (Miller, 2008 and references therein). Textures are central to investigating primary and secondary processes. Since this study focuses on the post-magmatic stage, fresh and altered rocks were selected for further study.

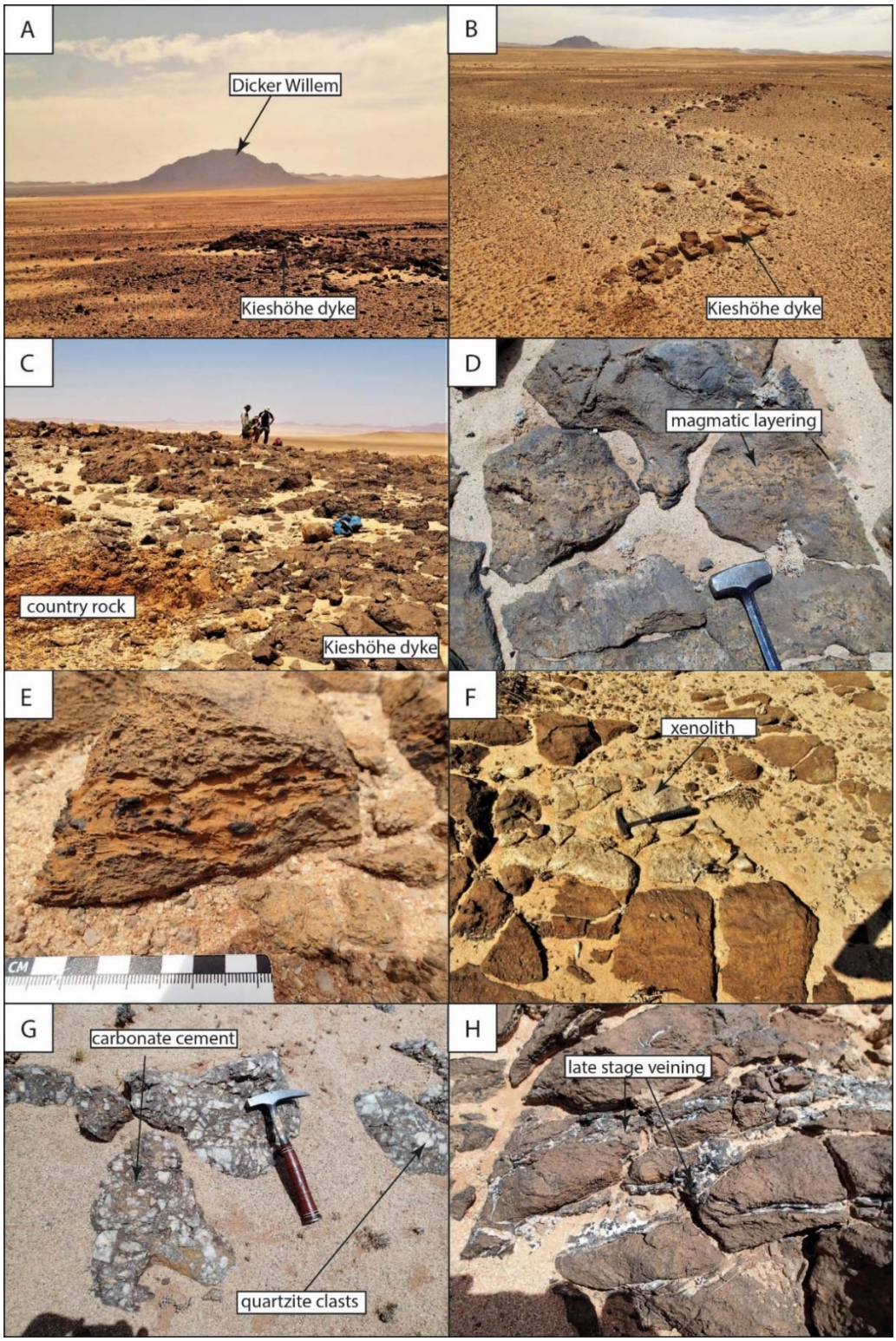

Figure 3. A) Spatial relationship between Dicker Willem (~20 km to the NE) and the Keishöhe carbonatite dykes, view looking north (NE pipe). B) The curvilinear attitude of dykes indicates a syn- to post magmatic sinistral shear (NE pipe). C) Contact between fenitised Namaqua Metamorphic Complex rocks and a ring dyke (Central pipe). D) Magmatic layering of magnetite in cone sheets (NE pipe). Layering is related to grain-size effects. E) Flow banding in NE pipe. F) Carbonatite dyke containing up to 1 m sized gneiss xenolith (Central pipe). G) Diatreme containing quartzite clasts cemented by fine-grained calcite and dolomite (SW pipe). H) Supergene alteration by secondary calcite veins and colloform Fe-Mn-oxide (Central pipe). All pictured dykes and sheets represent undifferentiated dolomite-calcite carbonatites.

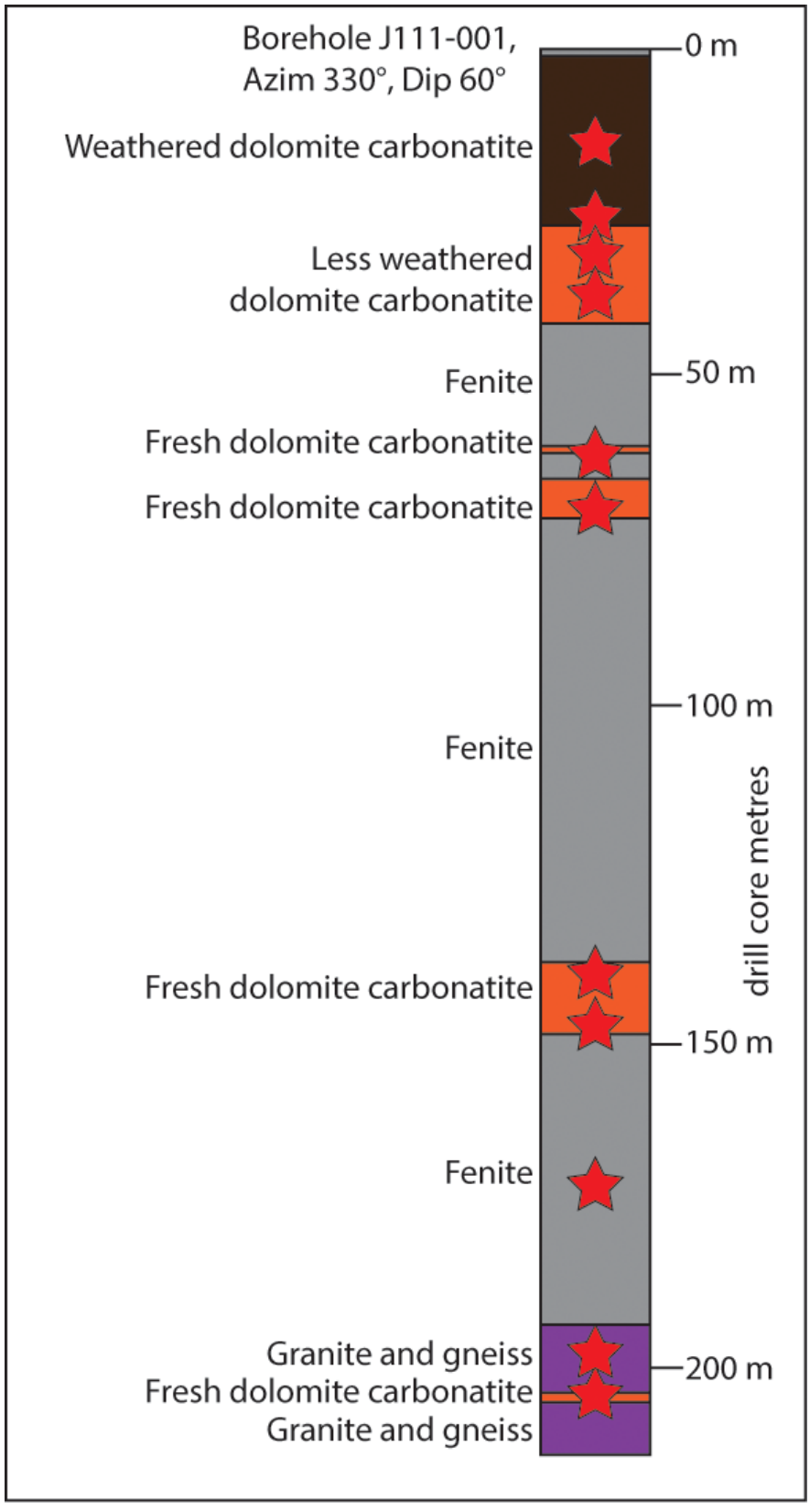

Figure 4. Core log of the deepest drill hole at Keishöhe. The drilling penetrated the 30° inclined carbonatite dyke with a dip of 60° and is therefore perpendicular to the wall rock contacts of the individual dykes. Red stars indicate sampling depths.

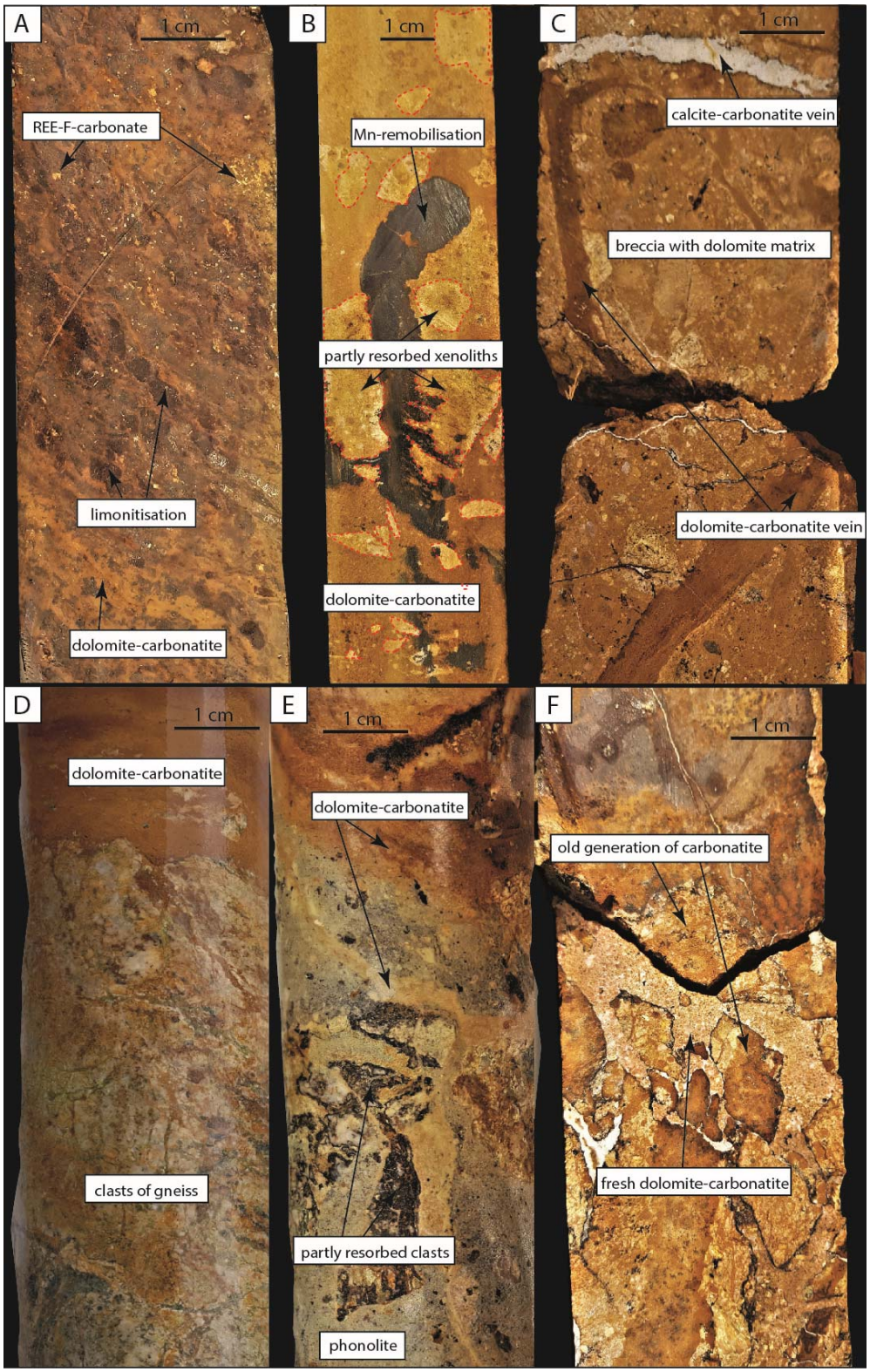

Figure 5. Drill core images of Keishöhe. A) Typical, carbonatite dyke of the uppermost, 40 m thick supergene alteration zone (J111-001, depth 17.4 m). B) Drill core (J111-001, depth 20.4 m) of a 20 m deep interval in a xenolith-rich dyke. Note supergene alteration by Mn phases. C) Cross-cutting relationship between xenolith-rich breccia, intruded by a dolomite-carbonatite and a calcite-carbonatite vein (150 m below surface; J111-001, depth 152.8 m). D) Dolomite-carbonatite dyke in gneiss of the Namaqua Group (J111-001, depth 181.2 m). E) Phonolite veins are fenitised and crosscut by a dolomite-carbonatite (J111-001, depth 194.3 m). Gneiss clasts from the Namaqua Metamorphic Complex are almost completely resorbed and replaced by mica. F) Multi-stage fine-grained dolomite-carbonatite breccia is common at Keishöhe (J111-001, depth 201.4 m).

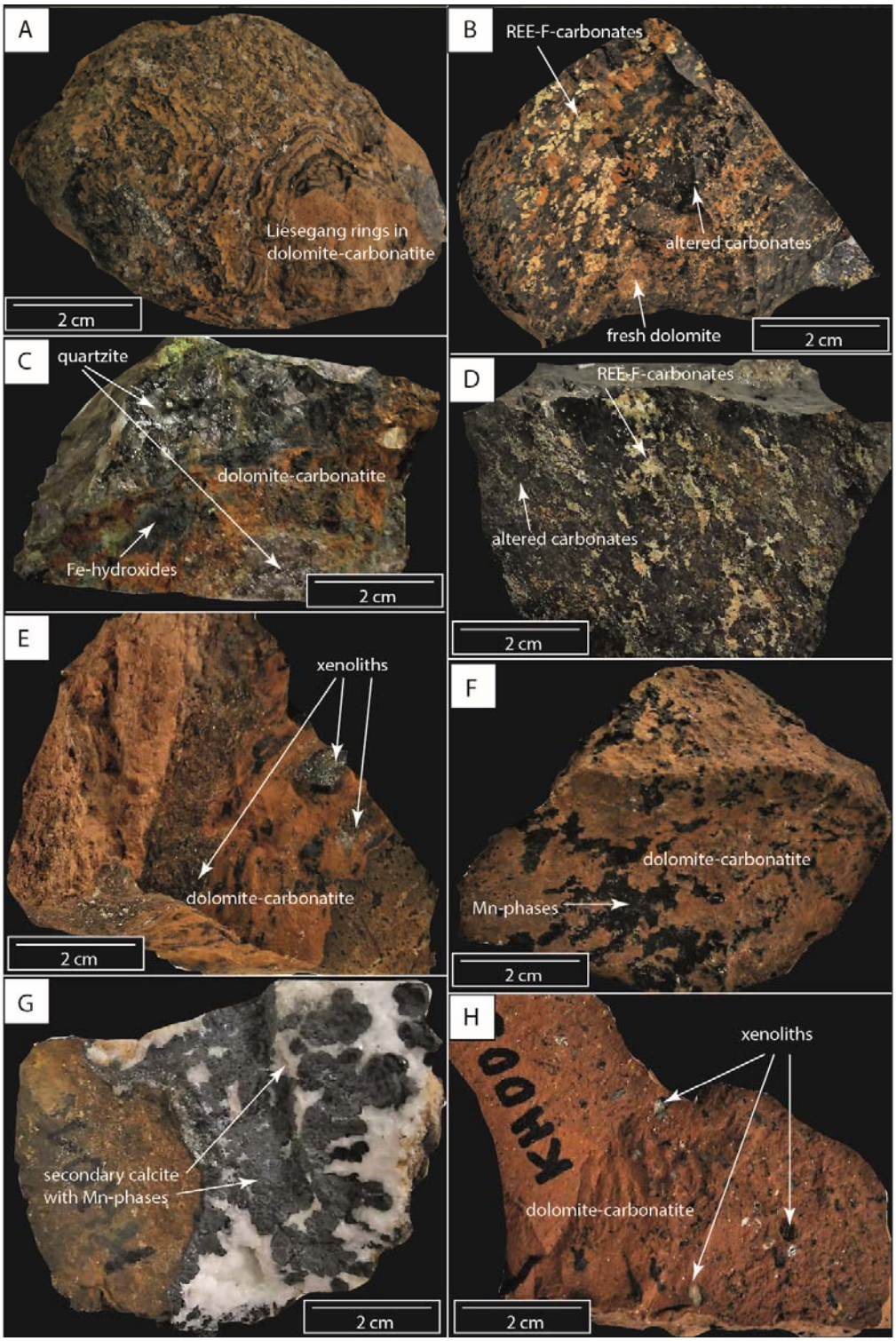

Figure 6. Representative samples from surface outcrops (scale for all samples 10 cm). A) Liesegang rings indicate supergene alteration. B) Dolomite-carbonatite dyke of the NE pipe. Note: This sample is xenolith-free. All yellow parts are intergrowths of REE-F-carbonates including synchysite and bastnäsite. C) Sample from a diatreme containing quartzite fragments from the Namaqua Metamorphic Complex lithologies cemented by fine-grained carbonatite. Primary magnetite and Fe-bearing carbonates are altered to goethite in the supergene alteration zone. D) Ankerite-carbonatite dyke with abundant yellow patches of REE-F-carbonates. E) Xenolith-rich dyke of the SW pipe. Note the apparent lack of REE-F-carbonate minerals. F) Supergene Mn-phase alteration in a diatreme sample of the NE pipe. G) Supergene calcite veinlets in karst. The Mn-phases show colloform textures indicative of supergene origin. H) Dyke rock of the Central pipe showing polylithic xenoliths of metamorphic rocks which are part of the Namaqua Metamorphic Complex, syenite clasts and rare mafic xenoliths, respectively.

Methods

Micro textures were studied by transmitted light microscopy and BSE imaging using a Vega Tescan Table-Top REM of the Oxford Instrument series (Chair of Petrology and Mineralogy, Karlsruhe Institute of Technology, Germany). An acceleration voltage of 15 kV and a beam current of 10 nA was used.

Whole-rock major and minor element geochemistry was done using wavelength dispersive XRF (S4 Explorer, Bruker) on fused beads (Li-tetraborate/-metaborate:sample ratio was 10:1) at the Laboratory for Environmental and Raw Material Analysis (LERA, KIT). CuK_{α}-radiation was used and the samples were scanned from 2° to 82° 2θ with an increment of 0.02° 2θ at 0.4 sec. The accuracy (between 1-6 %) was monitored by including the certified reference material (JDO-1, SY-2, PCC-1, SARM 5, RGM-1, AGV-1). Total sulphur (TS) and total carbon (TC) analyses were carried out with the Carbon-Sulphur-Analyser (CSA) CS-2000 from ELTRA. The accuracy (<0.2 %) and reproducibility was checked (<6 %) by correlation with certified reference materials (Steel, barium sulphate).

The trace element and REE-contents of the bulk samples were determined by ICP-MS (iCAP, Thermo Fisher Scientific) after HNO_3-HF-$HClO_4$-HCl acid digestion of powdered sample material (100 mg). To ensure complete silicate decomposition, 40 % HF (suprapure), 65 % $HClO_4$ (normatom) and the pre-oxidised (65 % HNO_3, subboiled) sample were heated in a closed Teflon vessel for 16 h at 120 °C. After evaporating the acids to incipient dryness, the residue was re-dissolved in 65 % HNO_3 (subboiled) and HCl (30 % normatom) and then evaporated three times to ensure purification. The final residue was again dissolved in 50 ml of ultrapure water. The precision of the ICPMS measurement was in the range of 1 %. Measurements are checked by regularly 5 µg/l standard solutions. The precision and the accuracy of the whole method including acid digestion was monitored by including the certified reference material CRM-Sy2 and GRE03 (High-Purity standards, Inc.) into the measurement sequence every ten samples (SD is between 1 % and 8 % for most elements).

Elemental distribution and macro textures in thin sections were investigated using the "area" mode of a Bruker Tornado M4 microXRF at the Mineralogical and Geochemical Micro-Analytical Laboratory (MAGMA Lab, Department of Applied Geochemistry, Technische Universität Berlin, Germany). Acceleration voltage was 50 kV using a beam current of 600 µA. Measuring point distance was 30 µm at 20 µm beam diameter. Measuring time was 60 ms per analysis spot. To obtain more precise data from a stronger signal, the analyses were run with two simultaneously operating spectrometers.

Results

Petrography of diatremes, sills and ring dykes

Calcite-carbonatite, dolomite-carbonatite, ankerite-carbonatite, diatreme breccia and minor phonolites occur at Keishöhe with a variable degree of hydrothermal/supergene and surficial alteration. Fenites at Keishöhe are strongly altered gneisses. However, only dolomite-carbonatite and the diatreme breccia were studied in detail in this contribution, since only those rocks provide sample material of sufficient quality. Calcite-carbonatite and ankerite-carbonatite are only mentioned in general, but not addressed in detail. Phonolites are generally not investigated.

Diatreme breccia

Diatreme breccias consist of clasts of country rocks (quartzite, gneiss, shale and sandstone; for description of the country rocks see Miller, 2008 and references therein). The clasts are cemented by a dolomite-carbonatite which is mineralogically different and therefore distinguished from the dolomite-carbonatite unit. Early apatite and monazite form euhedral grains up to 50 µm which grew at the contact between clast and carbonatitic matrix. Mica is formed on the margins of claystone clasts. Fe-rich dolomite occurs together with baryte as late phases, and minor vugs are filled by tiny euhedral quartz crystals. Dolomite is replaced by Fe-hydroxides in samples from the supergene zone and those taken close to the surface.

Dolomite-carbonatite

Most of the investigated carbonatite samples are dominated by Fe-bearing dolomite (>70 vol. %), with minor amounts of magnetite (< 5 vol. %), which classifies them as dolomite-carbonatite (after the classification of Gittins & Harmer, 1997). Dolomite-carbonatite samples from sheets and ring dykes are divided into xenolith-bearing and xenolith-free dolomite-carbonatites. While xenolith-rich samples show no macroscopically visible REE-mineralisation, xenolith-free samples are rich in REE-F-carbonates (up to 20 vol. %). Therefore, the different subtypes are classified as (I) REE-rich, xenolith-poor dolomite-carbonatite and (II) REE-poor, xenolith-rich carbonatite.

REE-rich, xenolith-poor samples

The primary REE-rich samples contain more than 50 vol. % of dolomite, ankerite (< 5 vol. %), accessory zircon and rare pyrochlore. Early apatite I is occasionally associated with monazite I. Magnetite is common and is usually enriched where flow banding is observed. Primary mica and pyroxenes are absent.

The alteration stage is characterised by a common intergrowth of REE-F-carbonates and secondary quartz, which only occurs in the altered samples. Both minerals occur in a fine-grained association whereas the REE-F-carbonates occur as needles intergrown with anhedral quartz. Occasionally (where the REE-F-carbonate – quartz intergrowth does not obscure any texture) a closely intergrown mineral assemblage of typically baryte, synchysite and bastnäsite completely replaces dihexagonal prismatic precursor minerals (up to 400 µm long; Fig. 7). Apatite I and monazite I occur next to these dihexagonal pseudomorphs and are strongly altered and partly replaced by a second generation of apatite II. However, their genetic relation to the REE-F-carbonate-intergrowths is unclear. The primary carbonates frequently show evidence of recrystallisation. Manganese oxides occasionally occur as the last minerals in this alteration association.

REE-poor, xenolith-rich samples

This subtype contains different xenoliths showing variable degrees of alteration. Quartzite xenoliths (Fig. 8A) show almost no evidence of alteration, whereas xenoliths of gneiss, alkali granite (Fig. 8B), syenite, which are all characterised by the presence of quartz (quartz I) and feldspars (Fig. 8C) contain mica (biotite) and pyroxene as alteration phases at carbonatite-xenolith contacts. Nevertheless, the xenolith-rich dolomite-carbonatite shows a primary mineral assemblage similar to the primary mineralogy of xenolith-free dolomite carbonatite with Fe-rich dolomite being the major carbonate phase. Early apatite I and monazite I occur occasionally in sizes between 10-50 µm. Occasionally, pyrochlore occurs.

Moreover, this carbonatite subtype also indicates the presence of primary dihexagonal minerals, which are pseudomorphically replaced by alteration phases (Fig. 8D-H). However, the abundance and type of alteration phases differ significantly. Alteration in this subtype is characterised by the lack of secondary REE-F-carbonate minerals. Dihexagonal pseudomorphic replacement textures which are present together with rare zircon (Fig. 8G) and corroded apatite I in altered samples consist of a mineral assemblage typified by a progressive sequence of Fe-dolomite II, baryte and very rare monazite II grains which occur as spheroids (Fig. 8E). Monazite II is however much more common in the REE-poor, xenolith-rich samples compared to the REE-rich samples and is present in the absence of the REE-F-carbonates, together with a second generation of Fe-bearing dolomite II.

These tiny monazite spheroids (~1µm) grew into open space of the pseudomorphs and represent the only REE mineral in the xenolith-rich carbonatite. Secondary quartz II is common and also present as intergrowths with secondary monazite II. Compared to xenolith-free samples the rare presence of monazite renders xenolith-rich samples almost REE-free. The primary Fe-bearing dolomite carbonates also show pervasive recrystallization.

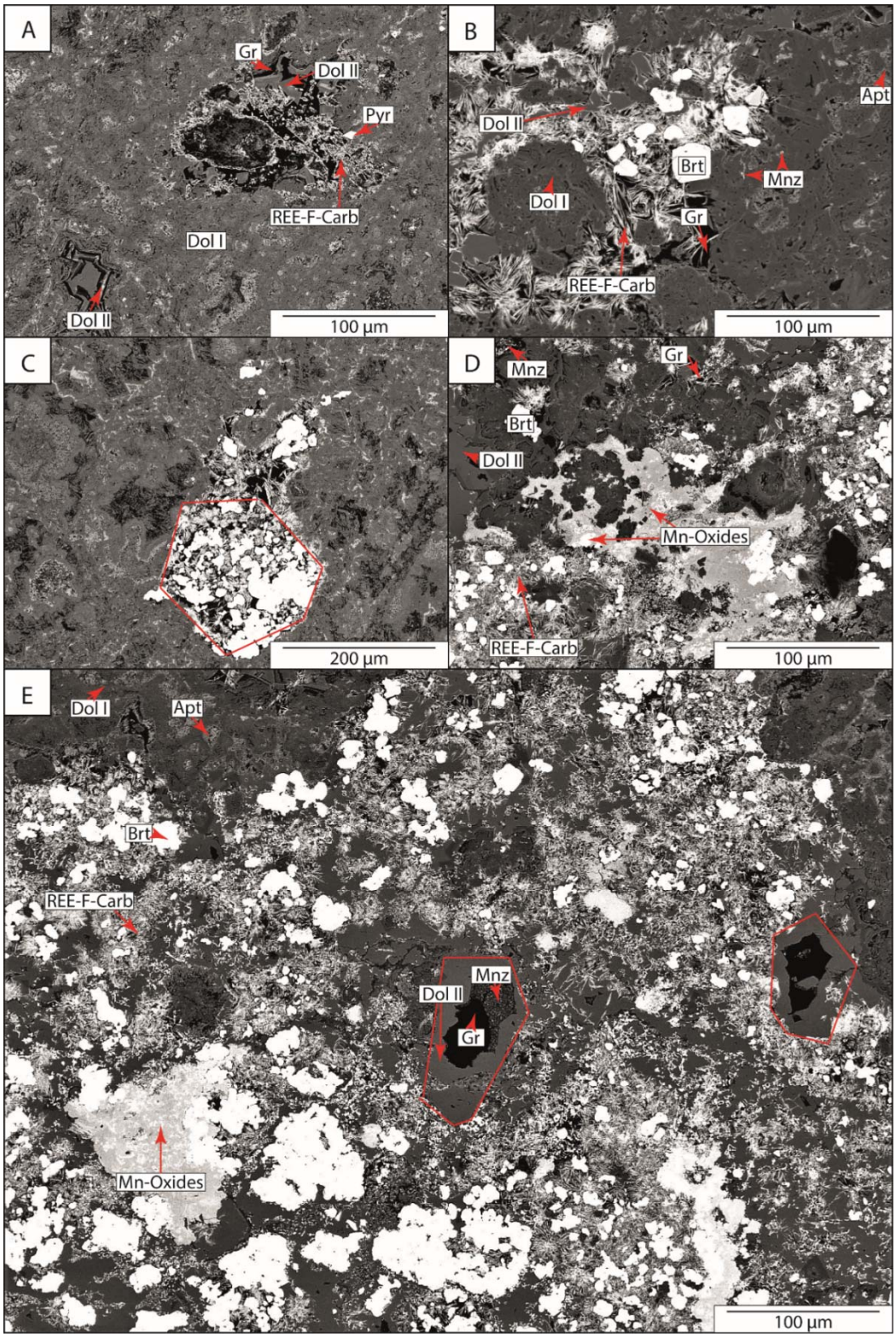

Figure 7. REE-rich, xenolith-poor dolomite-carbonatite (see Fig. 4F). A) While dolomite I (Dol I) dominates the rock, dolomite II (Dol II) only occurs in vugs. Pyrochlore (Pyr) occurs as a euhedral and accessory phase. B) First generation of monazite I (Mnz I) and apatite I (Apt I) occur in the early assemblage whereas REE-F-carbonates and baryte (Brt) occur in the hydrothermal/supergene alteration assemblage which fill dihexagonal pseudomorphs. C) Pseudomorph of an unidentified, dihexagonal prismatic crystal. D) Mn-oxides formed during the last stage of supergene alteration. E) Strongly hydrothermally/ supergene altered samples are generally baryte-rich.

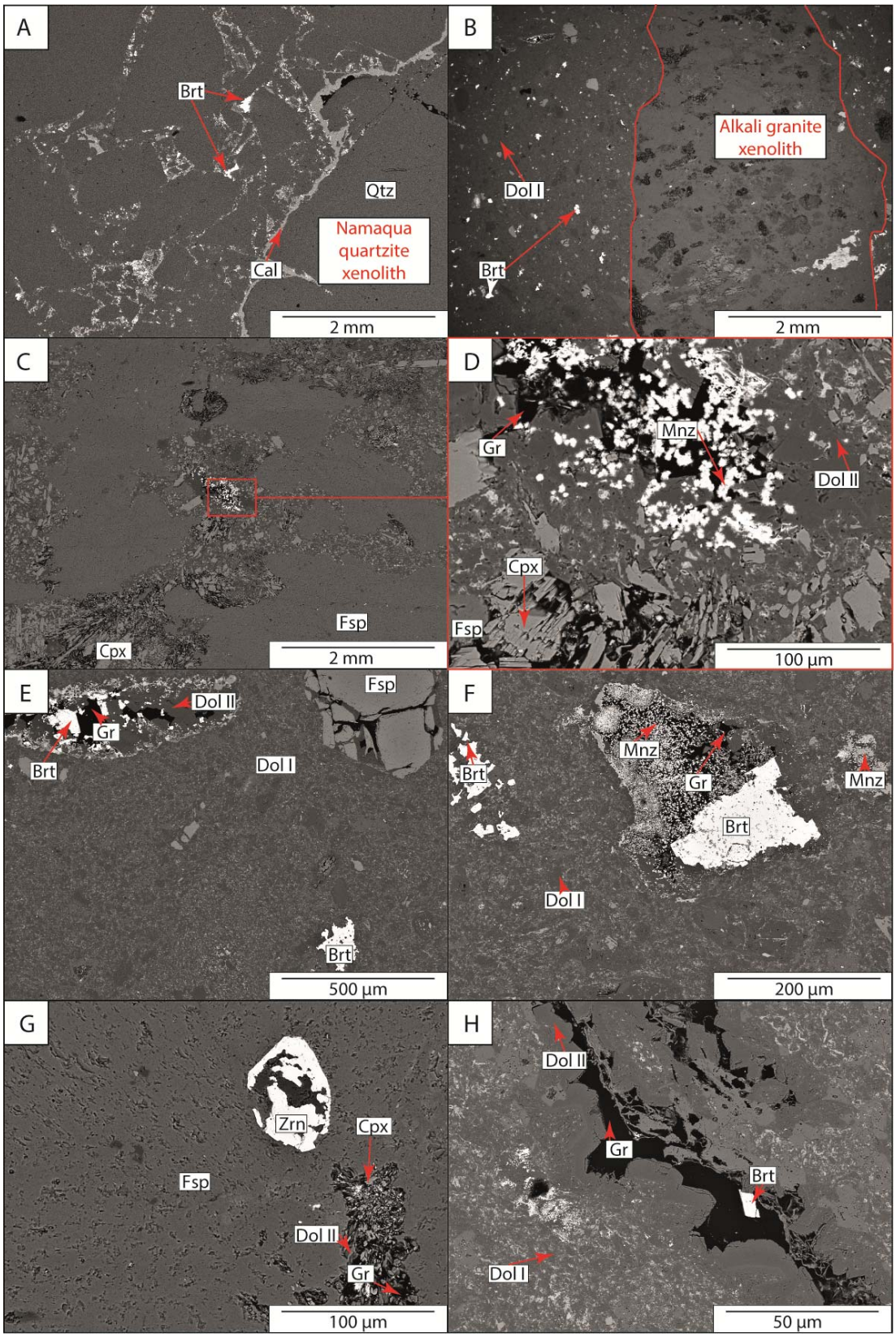

Figure 8. The REE-poor, xenolith-rich samples from drill cores and outcrops. (A) Clast supported quartzite breccia sample lacking REE-F-carbonates, baryte and calcite fillings on fractures. B) Alkali granite xenoliths composed of aegirine, feldspar and quartz in dolomite carbonatite. The xenolith is rounded and embayed indicating resorption during the magmatic stage. C-F) Pseudomorphic replacement textures after long-prismatic dihexagonal minerals filled with secondary spheroidal monazite, baryte and dolomite II. G) Zircon and feldspar grains are inherited xenocrystic phases. H) Baryte and dolomite II are often associated as vug fillings.

Micro XRF

MicroXRF scans provide detailed insight into element distribution at a thin section scale. Ten thin sections of REE-mineralised (xenolith-free, REE-rich subtype; Fig. 9) and barren (xenolith-rich, REE poor subtype, Fig. 10) dolomite-carbonatite were investigated. High contents of Mg (Fig. 9D), Fe (Fig. 9H) and P (Fig. 9I) in highly REE-mineralised samples reflect the presence of primary dolomite (yellow in Fig. 9C), Fe-oxides (magnetite) and apatite, respectively. The primary apatite I is REE-poor (Fig. 9K) and Sr-enriched (Fig. 9E). Secondary calcite II (orange in Fig. 9C & light blue in F) crosscutting primary dolomite I with Sr-poor margins (at the contact to REE-rich mineral zones; Fig. 9E, F & L). Element distribution maps indicate a strong association of REE and Si due to its significant correlation (Fig. 9G, K). This reflects the secondary REE-F-carbonate – quartz I intergrowths described in the petrography section. Ba-contents (Fig. 9J, L) that perfectly overlap sulphur contents (not shown in separate maps) demonstrate the exclusive mineralisation of Ba and S in secondary baryte, which occurs as a late-stage phase in vugs and along veinlets.

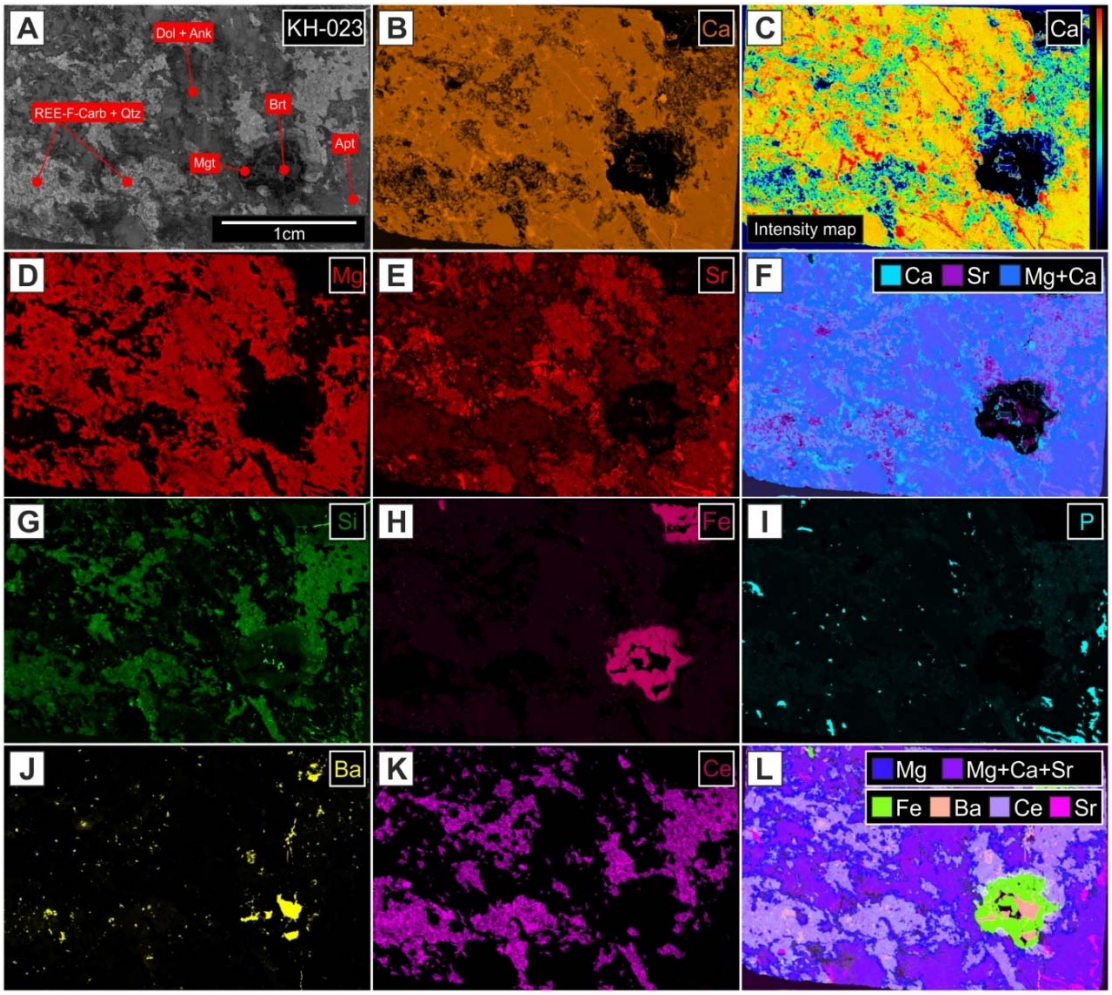

Figure 9. REE-rich, xenolith-free sample (KH-023) A) Greyscale overview image showing main mineral abundance. B) Calcium distribution. C) Calcium intensity map. D) Magnesium distribution. E) Strontium distribution. F) Combined Ca, Sr, Mg map. G) Silica distribution reflecting strong Si-REE intergrowth/quartz (Qtz) abundance. H) Iron distribution. Fe-content is mostly reflected as magnetite (Mgt) but is also abundant in dolomite (Dol) and ankerite (Ank), and forms tiny phases within the contact zone of REE minerals and quartz (not clearly visible in H due to normalisation effects). I) Phosphorus distribution reflecting apatite (Apt) abundance. J) Barium distribution. Sulphur shows the same distribution as Ba, which demonstrates the presence of baryte (Brt). K) Cerium distribution (representative for REE distribution) reflecting the REE-F-carbonate (REE-F-Carb) abundance. L) Combined Mg, Ca, Sr, Fe, Ce and Ba map.

In contrast, a combined evaluation of the Al and Si distribution (Fig. 10G & J), which indicates the presence of silicate xenoliths in barren carbonatite, reflects a clast abundance of up to 30 % of Namaqua Metamorphic Complex quartzite, strongly deformed gneiss, un-deformed syenite, alkali granite and unmeta-morphosed claystone reflecting variable Fe and Mg contents (Fig. 10D & H). In addition, Sr distribution maps demonstrate the presence of Sr-enriched dolomite clasts (Fig. 10B-F). The Mg distribution is mostly homogeneous with minor variations (Fig. 10D). Phosphorus distribution confirms the disseminated appearance (petrographically identified) of apatite grains (Fig. 10 I). Multi-element maps (Fig. 10L) combining Al (which shows identical distribution to K) and Si (besides others) confirm that large resorbed xenoliths (right side) show a complete transformation into mica (Fig. 10G, J & L). This is in contrast to Fe-rich clay stone xenoliths (lower left side; Fig. 10H & L) which show a Fe-hydroxide alteration rim (reflected by high Fe-concentrations) surrounding the corroded clast. The alkali granite clast in the upper left corner also shows an alteration rim around the clast and along grain boundaries that reflect an early stage of disaggregation. The REE distribution generally shows a relatively low abundance of REE-bearing minerals. REE concentrations are restricted to the secondary, hydrothermally or supergene REE phases between relictual carbonates (Fig. 10K).

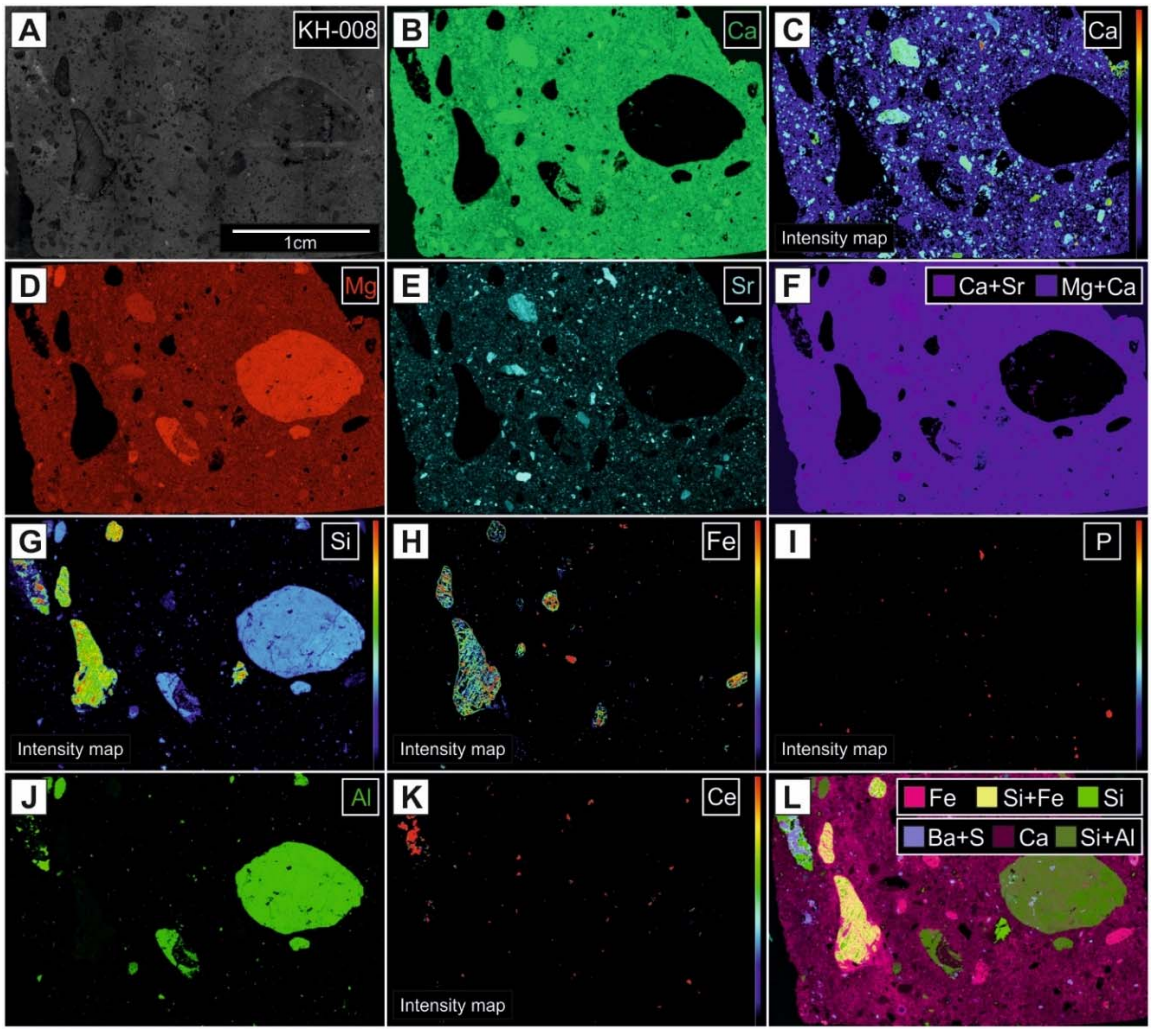

Figure 10. REE-poor, xenolith-rich sample (KH008) with a xenolith completely altered to mica on the right side of the images. A) Greyscale overview image. B) Calcium distribution. C) Calcium intensity map. D) Magnesium distribution. E) Strontium distribution. F) Combined Ca, Sr, Mg map. G) Silica intensity map. H) Iron intensity map. I) Phosphorous intensity map. J) Aluminum distribution (K shows an identical distribution). K) Cerium intensity map. D) Combined Fe, Ca, Si, Al, Ba and S map. Sulphur shows the same distribution as Ba, which demonstrates the presence of baryte. Note: Average La content is much lower compared to xenolith-free samples.

Whole rock geochemistry

The samples show different stages of hydrothermal and/or supergene alteration. The samples investigated (n=52) are classified according to their dominant carbonate mineralogy (Gittins & Harmer, 1997). This classification is supported by the whole rock geochemistry as (1) calcite-carbonatite (n= 11; Na_2O < 0.6 wt. %, Fe_2O_3 < 11.2 wt. %, MgO < 10.9 wt. %), (2) dolomite-carbonatite (n = 22; Na_2O < 0.4 wt. %, Fe_2O_3 < 16.0 wt. %, MgO < 15.3 wt. %) and (3) ankerite-carbonatite (n = 4; Na_2O < 1.3 wt. %, Fe_2O_3 < 25.8 wt. %, MgO < 19.3 wt. %). Five diatreme and fenite samples scatter widely in composition (Table 1). The phosphorous content is generally low (0.05-1.96 wt. %) but is equally low in both xenolith-rich and xenolith-free samples (Annex Table 1).

The carbonatites are relatively rich in Sr (0.1 to 0.6 wt. %) and Ba (up to 8.4 wt. %). Trace element contents of most elements are low. Elements such as Nb, Zr, Ta, which are often significantly enriched in carbonatites partly reach a maximum concentration of 0.2 wt. %. Occasionally, base metals such as Pb, Zn and Cu are enriched up to 0.2 wt. %.

TREE contents are variable and reach a maximum of 10 wt. % TREE with an average of 1.5 wt. % TREE reported in all lithologies. Lower TREE concentrations characterise the xenolith-rich samples (Fig. 11; Annex Tables 2 & 3). Samples rich in siliceous xenoliths (defined by Si content and carbon normalised Si content) show a clear REE depletion with increasing xenolith content. All investigated samples have typical LREE-enriched patterns (Fig. 11; Annex Tables 2 & 3). However, some samples (independent of the sample type) contain La + Ce ± Pr depletions which are not related to analytical artefacts (Fig. 11). Moreover, Sc reaches concentrations of up to 250 ppm. The reasons for these exotic REE patterns are not clear.

Discussion

The Keishöhe carbonatites as part of the Lüderitz Alkaline Province?

The Keishöhe hosts at least three carbonatite bodies and phonolites, with the latter only being recognised in some drill cores. The association of mineralised carbonatites and phonolites is commonly observed (e.g. Nabyl *et al.* 2020; Anenburg *et al.* 2021). Magmatism at Keishöhe remains undated (U-Pb age-dating of apatite failed due to high common lead contents in the studied samples). The carbonatites and alkaline rocks are situated only 10 km south of the 48 Ma Dicker Willem carbonatite complex (Fig. 2 and 11; Cooper & Reid, 1991). Together with the Teufelskuppe carbonatite, the Keishöhe and Dicker Willem carbonatite-alkaline complexes are hosted by the Kudu Lineament but the Keishöhe is located adjacent to the intersection of the Kudu Lineament and the Kuckaus-Poffader transcrustal Lineament (Fig. 2 and 11; Corner, 2000; Miller, 2008). Old transcrustal lineaments appear to be the major pathways for the ascent of alkaline silicate and carbonatitic magmas at most places worldwide (Banks *et al*. 2019).

Alkaline-carbonatite magmatism in the area is manifested by the ca. 1.1 Ga Namaqua Orogeny (Namaqua Metamorphic Complex), the ca. 130 Ma Lüderitz Alkaline Province and the ca. 46 Ma Klinghardt Mountains and Dicker Willem (Marsh *et al*. 2010). Besides Dicker Willem, there are more unstudied complexes hosted by, or related to, the Kudu Lineament and therefore named Kudu lineament complexes, comprising Dicker Willem carbonatite, Keishöhe carbonatite, Kaukausib carbonatite, Teufelskuppe and Karingarab carbonatite complexes. Based on the structural position of Keishöhe, the Keishöhe carbonatite complex likely belongs to the youngest event for which only Dicker Willem is dated.

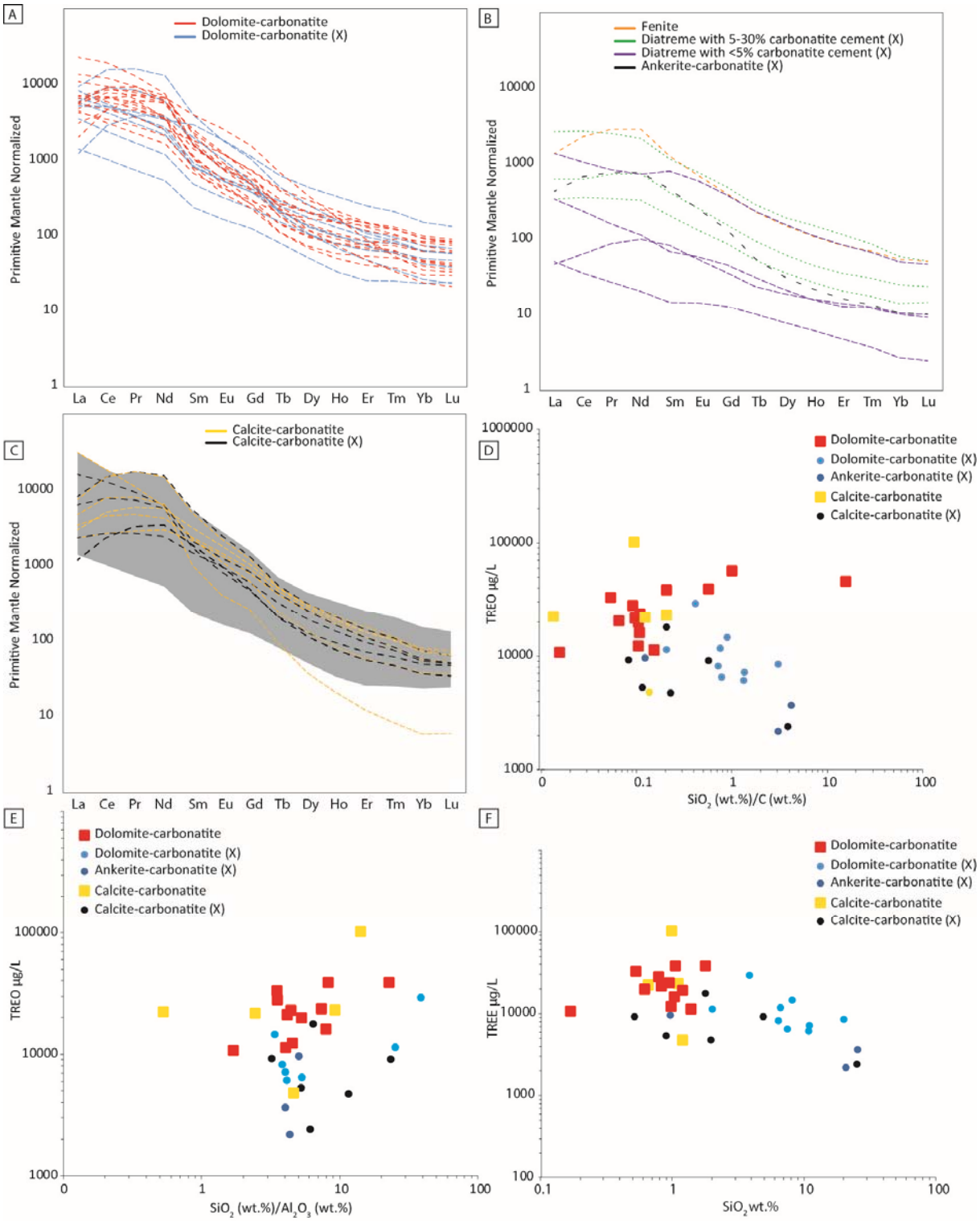

Figure 11. A) B) and C) Whole rock REE pattern. Samples marked with an X contain visible silicate rock xenoliths. Note some of the samples show uncommon REE patterns for carbonatites with La + Ce ± Pr depletions. Grey bar in C) represents the pattern of samples from figure A. D) TREE µg/L versus SiO_2-Carbon ratio (to exclude the dilution effect of the xenoliths in the whole rock). E) TREE µg/L versus SiO_2-Al_2O_3 ratio (to exclude the dilution effect of the Al-bearing xenoliths in the whole rock) F) SiO_2 wt. % versus TREE content. Note negative correlation with increasing Si-content in xenolith rich samples.

Due to the sparse geochronological data, some authors have come to different conclusions based on lithology. The Dicker Willem complex contains alkaline silicate rocks similar to those of the Lüderitz Alkaline Province, which may indicate a similar age (Cooper & Reid, 1991). The Lüderitz Alkaline Province (Granitberg, Pomona/Signalberg,

Drachenberg syenites and numerous alkaline dykes; Marsh, 1973, 1975a, b, 1976; Marsh *et al*. 2010) however lacks carbonatites and can therefore not easily be compared with the Kudu lineament carbonatite complexes. Although no precise age data are available for Keishöhe, it is spatially and structurally related (hosted by the Kudu lineament and ~ 10 km SE) to the 48 Ma Dicker Willem carbonatite (Cooper & Reid, 1991) and the other Kudu lineament carbonatite complexes. Nevertheless, all the Kudu lineament carbonatite complexes are hosted also by Namaqua Metamorphic Complex related structures that are crosscut by the Kudu lineament. Therefore, an older age cannot be excluded at this stage. The only known Namaqua Metamorphic Complex related carbonatite, namely the Glockenberg carbonatite, which is emplaced close to Dicker Willem (Walter *et al*. in prep.) is, however, strongly deformed, which has not so far been observed at Keishöhe. This feature tends to argue against a temporal relationship between the Keishöhe carbonatite complex and the metamorphic Glockenberg carbonatite.

If Keishöhe is temporally related to Dicker Willem, both carbonatite complexes belong to the Kudu lineament carbonatite event and not to the ~130 Ma Lüderitz Alkaline Province (Cooper & Reid, 1991). Based on this structural argument, a similar age has been inferred for the Teufelskuppe carbonatite by Verwoerd (1993) which would also add this intrusion to the discrete Kudu lineament carbonatite event. Further age-dating is required to demonstrate a common alkaline and carbonatite event on the Kudu lineament.

Marsh (1975a) explicitly excluded the 46 Ma Klinghardt phonolites and nephelinites from the Lüderitz Alkaline Province, because of a potential genetic relationship to an unrelated, widespread alkaline ultramafic event along the west coast of southern Africa (Dingle & Gentle, 1972; Moore, 1973). However, there are also arguments in favour of a much larger spread of the Lüderitz Alkaline Province, which also includes the inland of the Tsau-ǁKhaeb-(Sperrgebiet)-National Park where the Kudu lineament with the carbonatite complexes is located. It is not clear whether the alkaline rocks (mainly phonolites) at Dicker Willem and Keishöhe are part of the Lüderitz Alkaline Province or belong to a plume trace (Reid *et al*. 1990), or are related to the widespread alkaline ultramafic volcanic activity that occurred along the west coast during Paleocene to Eocene times (Moore, 1973; Dingle & Gentle, 1972).

The Lüderitz Alkaline Province (~130 Ma) and the phonolites of the Klinghardt Mountains (~46 Ma) are located on southern structures of the Namaqua belt (Reid *et al*. 1990; Marsh *et al*. 2010). Similar magmatic activity can be demonstrated for the northern side of the Namaqua belt, since the Gross Brukkaros volcanic complex (which also comprises carbonatite occurrences in the form of dyke swarms) has an Upper Cretaceous age (~75 Ma) and lies directly within the northern Namaqua orogeny front (Miller, 2008). The Namaqua Metamorphic Complex hosted Glockenberg carbonatite (25 km NNW of Keishöhe) follows an old shear zone parallel to the Excelsior-Lord Hill shear zone and is not situated on the Kudu Lineament. The fact that the Glockenberg is not situated on the Kudu lineament provides strong evidence that the framework of transcrustal lineaments (and not a single structure) are key to understanding the spatial relationships of the carbonatites in the area (Reid *et al*. 1990), whereas the temporal relationships indicate at least two maxima of magmatic activity during the breakup of the Atlantic Ocean in the late Cretaceous (Lüderitz Alkaline Province) and during the Eocene (Kudu lineament carbonatite complexes). The role of mantle plumes in southwestern Namibia is, however, not supported by offshore seamount traces. Therefore, more age dating in the area is required to unravel the genetic relationships of the isolated intrusions, dykes and volcanic cones.

Regarding the extent of the Lüderitz Alkaline Province and the recorded Eocene magmatic rocks, syenite and alkali granite xenoliths are noted at both Keishöhe and Dicker Willem, and very abundant syenitic and ultramafic xenoliths occur in the nephelinites on the Tsirub Farm (Nakashole *et al*. 2020) suggesting further extension of the ~130 Ma Lüderitz Alkaline Province to the east (at a deeper emplacement level) and is later transected by the Kudu lineament. It is suggested that the Kudu lineament carbonatite complexes incorporated clasts of the ~130 Ma alkaline rocks at depth during ascent and eruption.

In the context of the Tertiary land surface, the Keishöhe carbonatite (and the other Kudu lineament carbonatite complexes) represents a shallow level of the intrusion compared to those of the Lüderitz Alkaline

Province (with only intrusive rocks), whereas the xenolith record of the Keishöhe and Tsirub occurrences rather resemble the deeper levels of the potential extension of the Lüderitz Alkaline Province (> 600 m deeper in comparison to the outcrops at the coast, Fig. 13). The interpretation that the syenite complexes occur at deeper levels within the Namaqua Metamorphic Complex rocks fits nicely with the observed exhumed roof zone of the Granitberg nepheline syenite (located close to the coast and south of Lüderitz), and today is at an altitude of ~100 m.a.s.l., whereas Keishöhe is at about 750 m.a.s.l. (Marsh 1975). The occurrence of phonolite veins at Keishöhe, which are brecciated in the deeper levels, can be taken as a further indication of the genetic relationship, firstly to the nearby Dicker Willem carbonatite where similar phonolite dykes are observed, and secondly, to the numerous phonolite dykes of the Lüderitz Alkaline Province intruded during the Cretaceous, as well as the Eocene Klinghardt phonolites (see maps of Kaiser, 1926).

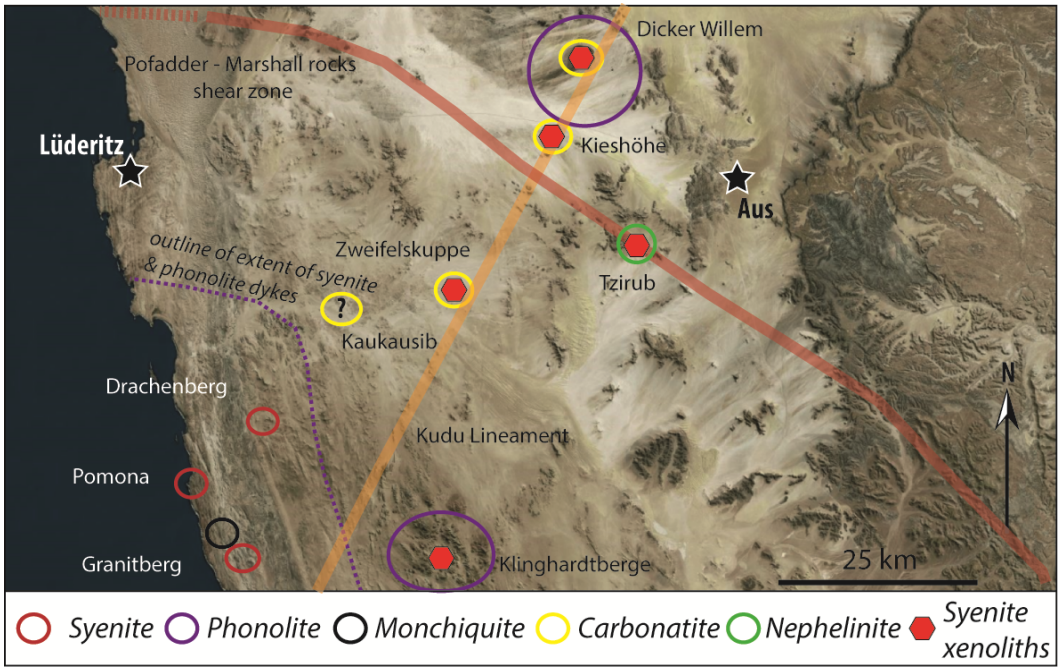

Figure 12. Satellite image of the Tsau-ǁKhaeb-(Sperrgebiet)-National Park with alkaline ignous rocks and carbonatites added (image taken from zoomearth.com). The framework of translithospheric lineaments (sketched) seems to be the major control for the distribution of the individual complexes.

The geometry of the Keishöhe carbonatite complex as indicator for a shallow emplacement

The ring dykes of Keishöhe are controlled by three intrusion centres. In general, ring dykes form as a consequence of magmatic doming (Mathieu *et al*. 2008) and sometimes by caldera formation or maar type eruptions (Kennedy & Stix, 2007). Hence, it is likely that Keishöhe has been eroded to a shallow subvolcanic level, only slightly below the former land surface. Marsh (1975a) observed that the end-Cretaceous-early-Tertiary land surface is transected by the Dicker Willem intrusion based on the observed Nama Group lithologies near the Splitterkuppe (Fig. 13). Dicker Willem is a subvolcanic intrusion which today occurs as a giant inselberg on the plains with the summit about 700 metres higher than Keishöhe. The Dicker Willem occurrence is very similar in geometry and rock types to the Khanneshin carbonatite volcano in Afghanistan which is almost not eroded (Tucker *et al*. 2012). Since only minor volumes of carbonatite are emplaced, and evidence for eruption is common (breccia pipes), we interpret the Keishöhe occurrence as a shallowly eroded maar-type volcano. The observation that Dicker Willem is situated at a higher topographic level and bears intrusive rocks, while the Keishöhe is less elevated above the plains but has a pronounced diatreme facies (extrusive character), requires a temporal discrepancy between the two magmatic occurrences.

Since carbonatites have a low viscosity and density, the occurrence of relatively large xenoliths (>1 m in diameter) in some of the carbonatite dykes and diatremes indicates a high ascent rate to enable such xenolith transport. The Fe-rich claystone clasts of recently eroded Nama Group (several hundred metres above the recent erosion level) observed in numerous samples indicate a downwards transport of Nama Group sedimentary material, further supporting a shallow emplacement depth. The discrepancy between the interpreted intrusion depths of the Dicker Willem and Keishöhe carbonatite complexes are better illustrated on Figure 13. Here we see the two scenarios which may explain the differences in intrusion style. There are no arguments available at the moment as to which of the two scenarios is the more likely. Either there has been vertical displacement through a major fault zone, or there has been significant doming resulting from the emplacement of Dicker Willem. This would explain the lack of Nama Group sediments between Splitterkuppe and the escarpment where the Nama Group lithologies occur east of Aus as remnants on the top of the mountains.

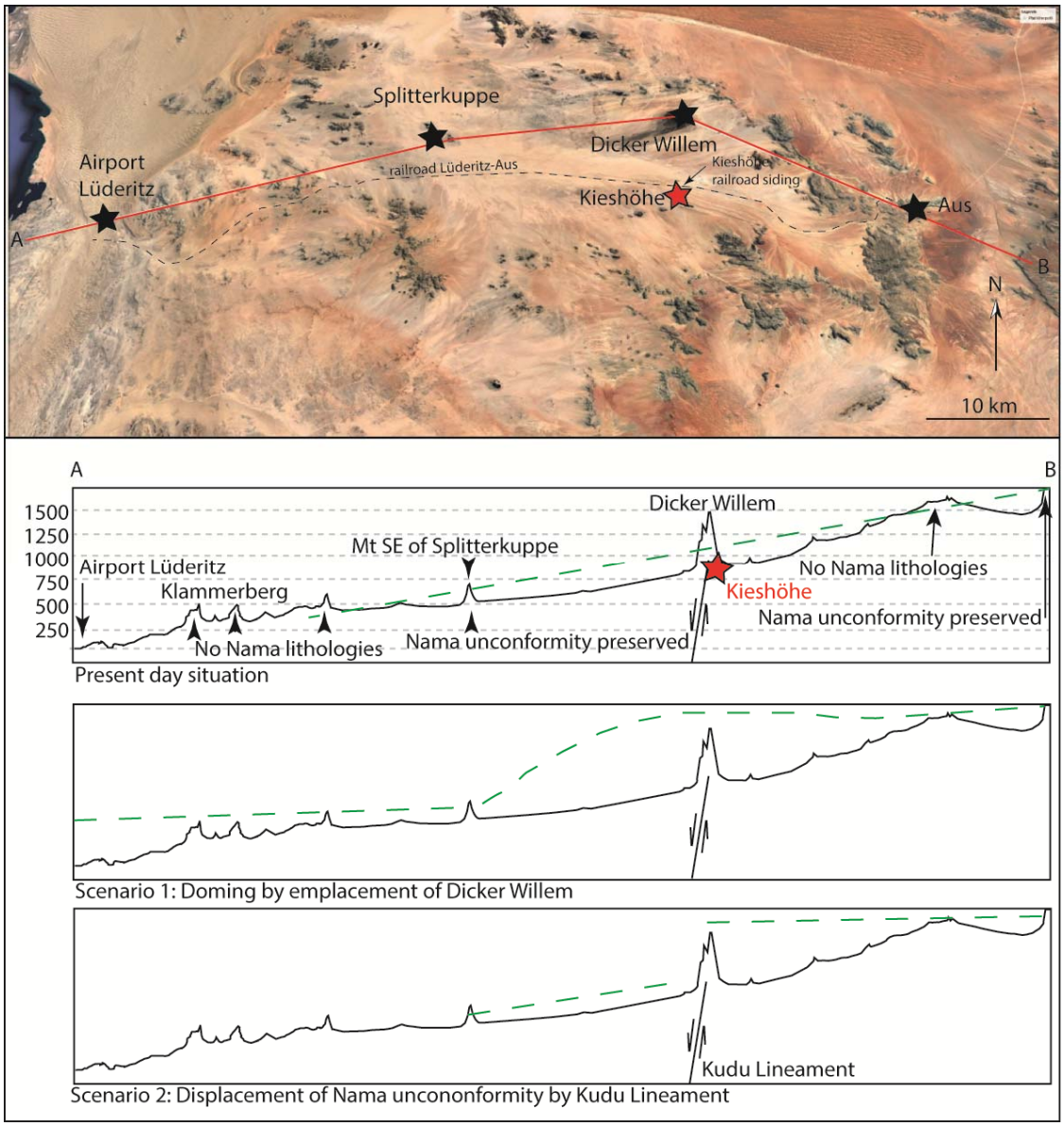

Figure 13. Interpretation of the emplacement depth at Keishöhe, Dicker Willem and Teufelskuppe (Twyfelskupje). Green lines indicate the Nama unconformity which needs to be displaced by either doming of Dicker Willem or by displacement at the Kudu Lineament to explain the Nama Group sediments at the elevation of Splitterkuppe and at the escarpment near Aus.

Transcrustal lineaments are one strong exploration indicators for the location of alkaline igneous rocks and carbonatites (Walter *et al*. 2021) amongst others (Banks *et al*. 2019). The northern front of the Namaqua belt is of particular interest, as the Excelsior-Lord Hill and the Pofadder shear zones form transcrustal lineaments which provide excellent pathways for melt ascent. Based on the work of Banks *et al*. (2019), the critical processes for REE and HFSE mineralisation in alkaline igneous rocks and carbonatites are fertility of the source, favourable lithospheric architecture and a geodynamic event. All of these critical processes are present in this province, namely a fertile source (evidenced by large amounts of alkaline rocks and carbonatites); favourable architecture for ascent of mantle melts (trans-crustal lineaments), and major geodynamic event/s with the ongoing opening of the Atlantic Ocean since the Cretaceous and potential plume activity (Reid *et al*. 1990).

Crustal contamination at Keishöhe

The general role of crustal contamination – magmatic vs. post-magmatic

Contamination may play an important role in carbonatite magma evolution (e.g., Anenburg *et al.* 2020; Chakhmouradian *et al*. 2008; Drüppel *et al*. 2005; Giebel *et al*. 2019b; Hode Vuorinen & Skelton, 2004; Wei *et al*. 2020) due to the high reactivity of volatile-rich carbonate melts and the large geochemical gradient with silicate wall rock and xenoliths. Some of the Keishöhe carbonatites contain large amounts of silicate xenoliths (between 10 and 70 vol. %). The effect of contamination by xenoliths is, of course, additionally dependent on the degree of xenolith absorption by the carbonate melt. This, in turn, is dependent on the time that elapses between xenolith entrainment and carbonatite solidification. This indicates that intrusions with fast cooling rates (mostly shallow intrusions), which are often characterised by fine-grained carbonatites, have a rather low potential to experience a strong magmatic contamination. In contrast, intrusions with slow cooling rates (mostly deeper intrusions) can partially or completely resorb the xenoliths.

A useful indicator of contamination in carbonatites is the increased presence of silicates. The abundance and stability of silicate minerals logically depends on silica solubility (<2.9 wt. % in carbonate melts at subvolcanic pressures; Weidendorfer *et al*. 2017) and silica activity, respectively. Both of these parameters are generally very low in carbonatite magmas. However, a continuous cycle of silicate crystallisation and silica contamination may lead to enhanced formation of silicate minerals such as mica and clinopyroxene (Barker, 2001; Giebel *et al*. 2019b; Massuyeau *et al*. 2015; Anenburg & Mavrogenes, 2018; Yarxley *et al*. 2022). The formation of mica furthermore requires the availability of Al. However, Al_2O_3 solubility (usually <1 wt. %) in carbonatite magmas is even lower than that of silica. Therefore, Al-rich lithologies are required to be assimilated. Indeed, syenite and gneiss xenoliths (both K-feldspar-bearing) at Keishöhe often show mica haloes, which are absent around quartzite xenoliths (Fig. 5E, F, 8A, 10).

Feldspar and quartz saturation, in contrast, usually cannot be reached during the magmatic stage of a carbonatite due to its low silica activity (Barker, 2001). It seems more likely that feldspar in the strongly contaminated dolomite-carbonatite is inherited from dis-aggregated Namaqua Metamorphic Complex gneiss xenoliths or alkaline granite xenoliths from the potential extension of the Lüderitz Alkaline Province, and/or formed during fenitisation. The occurrence of quartz in the Keishöhe carbonatites is, depending on the textures observed, evidence of either entrainment of xenocrysts, or of late-stage silicification during a post-magmatic hydro-thermal/supergene event. Rounded quartz I grains, which likely represent disaggregated, partly resorbed xenocrysts can be easily distinguished from quartz II, which is often euhedral and replaces magmatic stage minerals. These euhedral quartz II grains are likely of hydrothermal or supergene origin.

The effects of contamination must generally be distinguished within the magmatic and post-magmatic stages of a complex. Giebel *et al*. (2019b) have shown that an external silica introduction (by xenolith resorption) during the magmatic stage may cause increased REE incorporation into apatite due to the coupled britholite substitution ($Ca^{2+} + P^{5+} \rightarrow REE^{3+} + Si^{4+}$), which leads to the early removal of REEs from the carbonatite melt. As a result, these REEs cannot be further enriched in the melt,

and significantly less discrete REE minerals form in the more highly evolved magmas. This important consideration suggests that late-stage REE mineralisation may be inhibited by this process. This of course requires a sufficiently high concentration of P to allow apatite formation. However, P content and apatite occurrence, are generally very low at Keishöhe. The primary mineralogy of dolomite-carbonatite dykes and breccias (independent of the presence of xenoliths) of the Keishöhe furthermore suggests only low magmatic contamination effects. Even if the REE in xenolith-rich areas were more strongly incorporated in apatite due to magmatic contamination (as described by Giebel *et al*. 2019b) and therefore did not form larger quantities of discrete REE minerals (as might have been the case in xenolith-free areas) this would not explain the principally different REE contents in the whole rock data of the xenolith-rich and xenolith-free areas. Finally, REEs would be only incorporated into different minerals through this process, but are not principally enriched or depleted in the whole rock (as observed at Keishöhe). Therefore, a different explanation must be found for this observation.

Indeed, the dolomite carbonatites of Keishöhe show a marked post-magmatic overprint. This overprint is strongly dependent on the presence of xenoliths in the carbonatite. The investigated samples indicate that xenolith-rich portions, where silica was mobilised in a fluid through post-magmatic xenolith resorption, are REE depleted, while xenolith-free sections show significant post-magmatic quartz intergrowths with REE-F-carbonates (see negative correlation between REE and increasing xenolith-content; Fig. 11C, D, E). Accordingly, at least short-term mobilisation of the REE over undefined distances and enrichment of the REE by specific precipitation processes within the xenolith-free regions must have occurred. The fine intergrowth of REE-F-carbonates and quartz (Qtz II; Fig. 9G, K) as well as the common coexistence of REE-F carbonates and baryte (Fig.7E & 9 J) indicates a simultaneous transport and precipitation of REE, Si, S and Ba during late hydrothermal or supergene processes in the carbonatites of Keishöhe.

The effect of crustal contamination on post-magmatic REE-mineralisation

At hydrothermal or supergene conditions, the behaviour of REE in the presence of Si is not well constrained. However, Cui *et al*. (2020) demonstrated that the availability of silica has strong effects on sulphate solubility in fluids. In general, sulphur is a potential ligand which complexes with REEs in hydrothermal (and likely supergene) fluids. Recent modelling by Cui *et al*. (2020) even provides evidence that sulphate complexes demonstrate a stronger capacity to transport REE than chloride complexes in low temperature hydrothermal systems. In this situation, silica-saturated environments may support the efficiency of REE mobilisation, which increases significantly in Si saturated S-rich fluids (Cui *et al*. 2020). It is important to note that the experiments of Cui *et al.* (2020) are based on a simplified system. To confirm their applicability to natural carbonatite-associated systems, further studies with respect to more complex systems are necessary. Our observations on samples from Keishöhe show strong parallels to the results of Cui *et al.* (2020). Indeed, the occurrence of secondary baryte is one of the most obvious features of the hydrothermally or supergene altered samples that were studied. Thus, sulphur activity may play an important role in hydrothermal or supergene REE remobilisation at Keishöhe. Since the secondary mineral assemblage (REE-F-carbonates, baryte, quartz II, dolomite II, etc.) is stable over a wide range of physico-chemical conditions, it is not possible to distinguish between low-temperature hydrothermal (<100°) or supergene conditions without further data. Although the experiments by Cui *et al.* (2020) show a stronger effect of quartz saturation on the availability of sulphur in hydrothermal fluids at higher temperatures (above 330°C), even at lower temperatures there is a sufficiently strong effect that produces a significant positive influence on S solubility. Therefore, xenolith resorption may significantly influence REE mineralisation, not only at the magmatic stage (Giebel *et al*. 2019b), but also at the post-magmatic stage by hydrothermal and/or supergene processes.

The potential origin of REE and cause of variable REE mineralogy

The coexistence of baryte and REE minerals (especially REE-F-carbonates) within hydrothermal/supergene stage mineral assemblages is described from numerous other carbonatite occurrences as a typical mineral association for the replacement of burbankite (or carbocernaite; e.g. Giebel *et al*. 2017; Moore *et al*. 2015; Zaitsev *et al*. 1998). REE-F-carbonate-baryte assemblages of the REE-rich carbonatite subtypes as well as monazite-baryte assemblages of the REE-poor carbonatite subtypes appear as dihexagonal prismatic pseudomorphs which show the typical crystal form of burbankite. Therefore, it can be assumed that burbankite was present in the Keishöhe carbonatites as a primary mineral, which might serve as a potential REE source. Because both xenolith-rich and xenolith-free samples show evidence of the prior presence of burbankite (without noticeable differences in original burbankite abundance), it can be assumed that REE mineral dissolution and therefore REE remobilisation took place in both carbonatite subtypes. This renders it unlikely that simple REE oversaturation occurred only in the xenolith-free carbonatite subtype. In fact, it implies that the enhanced REE precipitation (as REE-F-carbonates) was not triggered only by remobilisation-induced REE oversaturation in the hydrothermal/supergene fluid, as this would be independent on the abundance of xenoliths. This, of course, does not exclude a temporary and local REE supersaturation of the fluid, presumably caused by the dissolution of the precursor REE mineral, but renders it of only minor importance for the entire REE mineralisation. Furthermore, it can be considered unlikely that pH gradients might act as a potential trigger for REE remobilisation/precipitation, since the pH of hydrothermal or supergene fluids is buffered in a carbonate-bearing rock. We suggested that REE mineralisation varies as an indirect result of variable REE-ligand stability due to variable silica concentrations in the hydrothermal/supergene fluid. In xenolith-free domains (REE-rich samples), the Si concentration in the fluid was too low to maintain a permanently high S solubility (see experiments by Cui *et al*. 2020). The decreasing Si content in the fluid was supported by quartz precipitation and may have led to simultaneous precipitation of baryte. The resulting decrease in S (lack of transport-ligand) in turn significantly reduced the ability of the fluid to mobilise REE over longer distances (by destabilisation of REE-S-complexes), and REE minerals precipitated indirectly due to the lack of dissolved Si. In contrast, within xenolith-rich samples (where xenolith resorption maintains continuous Si mobilisation) and in the presence of Si-saturated fluids, REEs are kept mobile by sulphur-complexes until REE get precipitated.

To explain the post-magmatic monazite (Mnz II) formation, an increased P content is required, which was probably provided by local apatite dissolution. In contrast to S, P serves as a binding ligand for REE, which favors the local formation of monazite (Giebel *et al*. 2017) independent of the formation of REE minerals by Si depletion in the fluid. This may explain the presence of monazite in both carbonatite subtypes. Preferably, monazite precipitated immediately where REE minerals have been dissolved. Therefore, monazites occur mainly directly in the pseudomorphs after burbankite. However, during replacement of the potential burbankite pseudomorphs, only minimal REE contents were immediately reprecipitated. Nevertheless, the occasional grains of monazite II in both the xenolith-rich and xenolith-free carbonatites (in particular in the latter subtype) are still negligible compared to the REE-F-carbonates in xenolith-free sections (Fig. 7). The source of the sulphur is not clear so far. However, recent studies by Walter *et al*. (2020) indicate a common S-enrichment in carbonatite-derived fluids. This implies, of course, that the original carbonatite melt itself already contained sulphur.

The extent of the impact of crustal contamination

The abundance of silicate xenoliths results in an increased potential for hydrothermal or supergene fluids to mobilise higher amounts of SiO_2 within the emplaced and crystallised carbonatite bodies. The disseminated nature of silicate xenoliths in the carbonatite promotes repetitive fluid - xenolith interaction which allows efficient Si-enrichment in the hydrothermal/supergene fluid over short distances. An exclusive/isolated fluid - wall-rock interaction with the adjacent country rock (without magmatically entrained and

distributed xenoliths) would probably have only a limited effect at the outermost margin of the carbonatite body due to the rapid precipitation of Si (typically as quartz at post-magmatic conditions), whereby the presence of xenoliths affects the entire carbonatite volume (as long as it is affected by xenolith entrainment) due to a dispersed Si-availability.

Conclusions

Silicate xenoliths – a hands on tool for REE-exploration in carbonatites?

The Keishöhe carbonatite complex contains both highly REE-mineralised, xenolith-free and poorly REE-mineralised, xenolith-rich dolomite-carbonatite dykes with variable degrees of alteration. The Keishöhe carbonatite complex is an impressive example of how silica contamination can influence both mobility but also grade of the REE mineralisation during hydrothermal/supergene alteration. Therefore, a proper evaluation of the potential occurrence and composition of xenoliths needs to be investigated early in an exploration programme. However, little is known, for example, about the influence of ironstones or BIFs (known from carbonatites of RSA) on the REE content of the finally emplaced carbonatite. More work is needed concerning the study of all aspects of crustal contamination on carbonatitic melts. The influence of contamination is complex, and the positive or negative influences on the REE enrichment during magmatic, hydrothermal and supergene processes need to be better understood in order to formulate definite proxies for mineral exploration.

This study demonstrates the need to evaluate the potential occurrence, composition and manner of xenoliths early during an exploration program. If the majority of the carbonatites in a complex contain resorbed or partly resorbed xenoliths of silicate wall rocks, the magma may become Si-enriched, which results in incorporation of REE into e.g. early apatite (same process observed by Giebel *et al*. 2019b). This, however, can have a significantly negative effect on any later enrichment processes because the REEs are removed early during the magmatic evolution. Thus, economic REE enrichment is unlikely when there is significant resorption at the early magmatic stage. Nevertheless, there are some counter examples such as Maoniuping which shows strong magmatic silica contamination but also one of the highest REE enrichments known in the world (Weng *et al*. 2022 and references therein). In contrast, the Keishöhe system has experienced a strong hydrothermal and/or supergene overprint which involves leaching of REEs from early magmatic REE-minerals (e.g. burbankite). During post-magmatic hydrothermal or supergene overprinting, xenolith- and Si-rich lithologies are more susceptible to secondary REE-remobilisation and subsequent enrichment. This is further dependent on the availability of sulphur, which may serve as a ligand for REE (Cui *et al*. 2020). Even though the specific experiments of Cui *et al.* (2020) only provide data about a highly simplified system, we see initial evidence in our observations that these experimental results have strong analogies to the much more complex systems of the Keishöhe. Of course, further work is needed to prove this conclusively.

A detailed understanding of hydro-thermal/supergene processes in a complex is essential for full evaluation. The sole recognition of silicate xenoliths in carbonatite does not allow a definite exploration decision to be made. Evidence of significant hydrothermal or supergene alteration of xenolith-bearing carbonatite is important for redirection of exploration from a magmatic REE deposit model towards a hydrothermal or supergene deposit model. Exploration tools must be adjusted.

Moreover, it has been shown that the major transcrustal structures in the Tsau-ǁKhaeb-(Sperrgebiet)-National Park provide a lithospheric architecture and mappable framework for the location of carbonatites or similar mantle-derived magmatic silicate rocks. These rocks are today highly prospective for REE ores. In this region, numerous geophysical anomalies (Miller, 2008) are hidden by a few metres of cover meaning that further discoveries are likely to be made in the area.

Acknowledgements

The Keishöhe carbonatite is situated within the Tsau-ǁKhaeb-(Sperrgebiet)-National Park in southern Namibia and is located on Exploration Prospecting License (EPL) 4458. This license was granted by the Namibian Ministry of Mines and Energy to Bonya Resources Pty Ltd, a subsidiary of the Shali Group. We thank Wilhelm Shali, Executive Chairman of the Shali Group for providing access to the EPL, to the drill cores and for assistance with administrative work including sample export. Emmanuel Shilongo, Andreas Stiehler and Jack Palmer are thanked for insightful discussions during fieldwork. Furthermore, we thank Helke Mocke for editorial guidance. Michael Anenburg and an anonymous reviewer are thankfully acknowledged for their constructive feedback. Greg Symons and Klaus Brauch (Terratec Namibia) as well as Anna Nguno (Ministry of Mines and Energy) are thankfully acknowledged for help with some of the logistics and administration. Ingrid Stengel (Geological Society of Namibia) is thanked for providing us with the opportunities to present our ongoing work to the geological community in Namibia. Elisabeth Eiche, Beate Ötzel, Claudia Mössner, David Schiebel, Kristian Nikoloski (all LERA facilities, KIT) are thanked for their analytical and preparation support. We are thankful to the German Science Foundation (DFG) for financial support (grant WA 3116/4-1).

References

Anenburg, M. & Mavrogenes, J.A. 2018. Carbonatitic versus hydrothermal origin for fluorapatite REE-Th deposits: Experimental study of REE transport and crustal "antiskarn" metasomatism. *American Journal of Science*, **318** (**3**), 335-366. https://doi.org/10.2475/03.2018.03

Anenburg, M., Mavrogenes, J.A., Frigo, C. & Wall, F. 2020. Rare earth element mobility in and around carbonatites controlled by sodium, potassium, and silica. *Science Advances*, **6** (**41**), 1-10, eabb6570.

Anenburg, M., Broom-Fendley S., & Chen W. 2021. Formation of Rare Earth Deposits in Carbonatites. *Elements* **17** (**5**), 327-332. https://doi.org/10.2138/gselements.17.5.327

Banks, G.J., Walter, B.F., Marks, M.A. & Siegfried, P.R. 2019. Defining an alkaline igneous-associated REE-HFSE mineral system: a foundation to map plays, uncertainty and risks to project value. *Minerals*, **(9) 97**, 1-28. https://doi.org/10.3390/min9020097

Barker, D.S. 2001. Calculated silica activities in carbonatite liquids. *Contributions to Mineralogy and Petrology*, **141**, 704-709.

Bell, K. & Simonetti, A. 2010. Source of parental melts to carbonatites–critical isotopic constraints. *Mineralogy and Petrology*, **98** (**1**), 77-89.

Berkesi, M., Bali, E., Bodnar, R.J., Szabó, Á. & Guzmics, T. 2020. Carbonatite and highly peralkaline nephelinite melts from Oldoinyo Lengai Volcano, Tanzania: The role of natrite-normative fluid degassing. *Gondwana Research*, **85**, 76-83.

Broom-Fendley, S., Brady, A.E., Wall, F., Gunn, G. & Dawes, W. 2017. REE minerals at the Songwe Hill carbonatite, Malawi: HREE-enrichment in late-stage apatite. *Ore Geology Reviews*, **81**, 23-41.

Castor, S.B. 2008. The Mountain Pass rare-earth carbonatite and associated ultrapotassic rocks, California. *Canadian Mineralogist*, **46** (**4**), 779-806.

Chakhmouradian, A.R., Mumin, A.H., Demény, A. & Elliott, B. 2008. Postorogenic carbonatites at Eden Lake, Trans-Hudson Orogen (northern Manitoba, Canada): geological setting, mineralogy and geochemistry. *Lithos*, **103** (**3-4**), 503-526.

Chakhmouradian, A.R. & Wall, F. 2012. Rare earth elements: minerals, mines, magnets (and more). *Elements*, **8** (**5**), 333-340.

Chakhmouradian, A.R. & Zaitsev, A.N. 2012. Rare earth mineralization in igneous rocks: sources and processes. *Elements*, **8** (**5**), 347-353.

Chikanda, F., Otake, T., Ohtomo, Y., Ito, A., Yokoyama, T.D. & Sato, T. 2019. Magmatic-hydrothermal processes associated with rare earth element enrichment in the Kangankunde Carbonatite Complex, Malawi. *Minerals*, **9** (**7**), **442**, 1-22.

Cooper, A.F. 1988. Geology of Dicker Willem, a subvolcanic carbonate complex in South-West Namibia. *Communications of the*

Geological Survey of South West Africa / Namibia, **4**, 3-12.

Cooper, A.F. & Reid, D.L. 1991. Textural evidence for calcite carbonatite magmas, Dicker Willem, southwest Namibia. *Geology*, **19** (**12**), 1193-1196.

Corner, B. 2000. Crustal framework of Namibia derived from magnetic and gravity data. *Communications of the Geological Survey of South West Africa / Namibia*, **12**, 13-19.

Cui, H., Zhong, R., Xie, Y., Yuan, X., Liu, W., Brugger, J. & Yu, C. 2020. Forming sulfate- and REE-rich fluids in the presence of quartz. *Geology*, **48** (**2**), 145-148.

Dalton, J.A. & Presnall, D.C. 1998. The continuum of primary carbonatitic–kimberlitic melt compositions in equilibrium with lherzolite: data from the system CaO–MgO–Al_2O_3–SiO_2–CO_2 at 6 GPa. *Journal of Petrology*, **39** (**11-12**), 1953-1964.

Dietzel, C.A., Kristandt, T., Dahlgren, S., Giebel, R.J., Marks, M.A., Wenzel, T. & Markl, G. 2019. Hydrothermal processes in the Fen alkaline-carbonatite complex, southern Norway. *Ore Geology Reviews*, **111**, article 102969.

Dingle, R. & Gentle, R.I. 1972. Early Tertiary volcanic rocks on the Agulhas Bank, South African Continental Shelf. *Geological Magazine*, **109**, 1 27 - 1 36.

Drüppel, K., Hoefs, J. & Okrusch, M. 2005. Fenitizing processes induced by ferrocarbonatite magmatism at Swartbooisdrif, NW Namibia. *Journal of Petrology*, **46** (**2**), 377-406.

Edahbi, M., Plante, B., Benzaazoua, M., Kormos, L. & Pelletier, M. 2018. Rare earth elements (La, Ce, Pr, Nd, and Sm) from a carbonatite deposit: Mineralogical characterization and geochemical behavior. *Minerals*, **8** (**2**), 55.

Elliott, H., Wall, F., Chakhmouradian, A., Siegfried, P., Dahlgren, S., Weatherley, S., Finch, A., Marks, M., Dowman, E. & Deady, E. 2018. Fenites associated with carbonatite complexes: A review. *Ore Geology Reviews*, **93**, 38-59.

Gendron, L., Bis, R. & Rodrigue, M. 1984. Underground mining and pyrochlore ore processing at Niobec mine, Quebec, Canada. *In*: Stuart, H. (Ed.) *Niobium, Proceedings of the International Symposium Metallurgical Society AIME (American Institute of Mining, Metallurgical and Petroleum Engineers).* Warrendale, Pennsylvania, pp. 79-96.

Giebel, R.J., Gauert, C.D.K., Marks, M.A.W., Costin, G. & Markl, G. 2017. Multi-Stage formation of REE Minerals in the Palabora Carbonatite Complex, South Africa. *American Mineralogist*, **102** (**6**), 1218-1233.

Giebel, R.J., Marks, M.A.W., Gauert, C.D.K. & Markl, G. 2019a. A model for the formation of carbonatite-phoscorite assemblages based on the compositional variation of mica and apatite from the Palabora Carbonatite Complex, South Africa. *Lithos*, **324-325**, 89-104.

Giebel, R.J., Parsapoor, A., Walter, B., Braunger, S., Marks, M.A.W., Wenzel, T. & Markl, G. 2019b. Evidence for magma – wall rock interaction in carbonatites from the Kaiserstuhl Volcanic Complex (Southwest Germany). *Journal of Petrology*, **60**, 1163-1194.

Gittins, J. & Harmer, R.E. 1997. What is ferrocarbonatite? A revised classification. *Journal of African Earth Sciences*, **25** (**1**), 159-168.

Goodenough, K.M., Wall, F. & Merriman, D. 2018. The rare earth elements: Demand, global resources, and challenges for resourcing future generations. *Natural Resources Research*, **27** (**2**), 201–216. https://doi.org/10.1007/s11053-017-9336-5

Hode Vuorinen, J.H. & Skelton, A.D. 2004. Origin of silicate minerals in carbonatites from Alnö Island, Sweden: magmatic crystallization or wall rock assimilation? *Terra Nova*, **16**, 210-215.

Humphreys-Williams, E.R. & Zahirovic, S. 2021. Carbonatites and global tectonics. *Elements*, **17** (**5**), 339-344.

Ivanyuk, G.Y., Kalashnikov, A., Pakhomovsky, Y.A., Mikhailova, J., Yakovenchuk, V., Konopleva, N., Sokharev, V., Bazai, A. & Goryainov, P. 2016. Economic minerals of the Kovdor baddeleyite-apatite-magnetite deposit, Russia: Mineralogy, spatial distribution and ore processing optimization. *Ore Geology Reviews*, **77**, 279-311.

Jackson, M.P. 1976. *High-grade Metamorphism and Migmatization of the Namaqua Metamorphic Complex around Aus in the Southern Namib Desert, South West Africa*. University of Cape Town, Department of Geology, 299 pp.

Kaiser, E. 1926. *Die Diamantenwüste Sudwestafrikas*, Volume I. Dietrich Reimer, Berlin, 321 pp. 4 plates, 13 maps.

Kennedy, B. & Stix, J. 2007. Magmatic processes associated with caldera collapse at

Ossipee ring dyke, New Hampshire. *Geological Society of America Bulletin*, **119** (**1-2**), 3-17.

Kröner, A. 1973. Comments on "Is the African plate stationary?" *Nature*, **243**, 29-30.

Kynicky, J., Smith, M.P. & Xu, C. 2012. Diversity of rare earth deposits: the key example of China. *Elements*, **8** (**5**), 361-367.

Le Maitre, R., Streckeisen, A., Zanettin, B., Le Bas, M., Bonin, B., Bateman, P., Bellieni, G., Dudek, A., Efremova, A. & Keller, J. 2002. *Igneous rocks. A Classification and Glossary of Terms. Recommendations of the IUGS Subcommission on the Systematics of Igneous Rocks*. Cambridge University Press, Cambridge, xvi + 236 pp.

Lee, W.-J. & Wyllie, P.J. 1994. Experimental data bearing on liquid immiscibility, crystal fractionation, and the origin of calciocarbonatites and natrocarbonatites. *International Geology Review*, **36**, 797-819.

Lock, B.E. & Marsh, J. 1981. Tertiary phonolite volcanism in the Klinghardt mountains of South West Africa/Namibia. *South African Journal of Geology*, **84** (**1**), 1-6.

Lottermoser, B.G. 1990. Rare-earth element mineralisation within the Mt. Weld carbonatite laterite, Western Australia. *Lithos*, **24** (**2**), 151-167.

Mariano, A.N. 1989. Nature of economic mineralization in carbonatites and related rocks. *In*: Bell, K. (Ed.) *Carbonatites: Genesis and Evolution*, London, UK: Unwin Hyman, pp. 149-176.

Marlow A.G. & Palmer M.R. in press. The REE-Enriched Twyfelskupje Carbonatite Complex, Southern Namibia. Submitted to Economic Geology.

Marsh, J.S. 1973. *Alkaline Igneous Rocks of the Coastal Belt, South of Lüderitz, South West Africa: a Petrological Study*. Unpublished Ph.D. Thesis, Cape Town, 285 pp.

Marsh, J.S. 1975a. The Lüderitz Alkaline Province, South West Africa I: descriptive petrology of the Granitberg Foyaite complex. *South African Journal of Geology*, **78** (**2**), 215-224.

Marsh, J.S. 1975b. The Lüderitz Alkaline Province, South West Africa II: metasomatism and assimilation in the contact aureole of the Granitberg Foyaite complex. *South African Journal of Geology*, **78** (**2**), 225-233.

Marsh, J.S. 1976. The Lüderitz alkaline province, South West Africa, III: The Pomona and Drachenberg Syenite Complexes. *South African Journal of Geology*, **79** (**2**), 168-176.

Marsh, J.S. 1987. Evolution of a strongly differentiated suite of phonolites from the Klinghardt Mountains, Namibia. *Lithos*, **20**, 41-58.

Marsh, J.S., Phillips, D. & Lock, B.E. 2010. $^{40}Ar/^{39}Ar$ dating of the Klinghardt and Stalhart Phonolites, Namibia, and Comments on the Evolution of the Klinghardt Volcanic Field. *Communications of the Geological Survey of Namibia*, **20**, 1-8.

Massuyeau, M., Gardés, E., Morizet, Y. & Gaillard, F. 2015. A model for the activity of silica along the carbonatite–kimberlite–mellilitite–basanite melt compositional joint. *Chemical Geology*, **418**, 206-216.

Mathieu, L., De Vries, B.V.W., Holohan, E.P. & Troll, V.R. 2008. Dykes, cups, saucers and sills: Analogue experiments on magma intrusion into brittle rocks. *Earth and Planetary Science Letters*, **271** (**1-4**), 1-13.

Miller, R. 2008. *The Geology of Namibia* (Volumes 1-3). Ministry of Mines and Energy, Namibia, Geological Survey.

Mitchell, R.H. 2005. Carbonatites and carbonatites and carbonatites. *Canadian Mineralogist*, **43** (**6**), 2049-2068.

Moore. A.E. 1973. The olivine melilitite-kimberlite association of Namaqualand. *International Kimberlite Conference, Extended Abstracts*, South Africa, pp. 239-242. https://doi.org/10.29173/ikc895.

Moore, K.R. & Wood, B.J. 1998. The transition from carbonate to silicate melts in the CaO-MgO-SiO2-CO2 system. *Journal of Petrology*, **39** (**11-12**), 1943-1951.

Moore, M., Chakhmouradian, A.R., Mariano, A.N. & Sidhu, R. 2015. Evolution of rare-earth mineralization in the Bear Lodge carbonatite, Wyoming: Mineralogical and isotopic evidence. *Ore Geology Reviews*, **64**, 499-521.

Nabyl, Z., Massuyeau, M., Gaillard, F., Tuduri, J., Iacono-Marziano, G., Rogerie, G., Le Trong, E., Di Carlo, I., Melleton, J. & Bailly, L. 2020. A window in the course of alkaline magma differentiation conducive to immiscible REE-rich carbonatites. *Geochimica et Cosmochimica Acta,* **282**, 297-323. https://doi.org/10.1016/j.gca.2020.04.008

Nakashole, A., le Roex, A. & Reid, D. 2020. Geochemistry and petrogenesis of the Tsirub nephelinite intrusions, southern Namibia.

Journal of African Earth Sciences, **162**, 103701.

Reid, D.L., Cooper, A.F., Rex, D.C. & Harmer, R.E. 1990. Timing of post-Karoo alkaline volcanism in southern Namibia. *Geological Magazine*, **127** (**5**), 427-433.

Shilongo, E. 2014. Shali Group Internal Report| Nov. 2014, Pages 25, 27.

Smith, M.P., Campbell, L.S. & Kynicky, J. 2015. A review of the genesis of the world class Bayan Obo Fe–REE–Nb deposits, Inner Mongolia, China: multistage processes and outstanding questions. *Ore Geology Reviews*, **64**, 459-476.

Stocken, C.G. 1978. *A Review of the Later Mesozoic and Cenozoic Deposits of the Sperrgebiet*. Unpublished Report, Geological Department, Consolidated Diamond Mines of South West Africa (Pty) Ltd, pp. 1-33.

Tucker, R.D., Belkin, H.E., Schulz, K.J., Peters, S.G., Horton, F., Buttleman, K. & Scott, E.R. 2012. A major light rare-earth element (LREE) resource in the Khanneshin carbonatite complex, southern Afghanistan. *Economic Geology*, **107** (**2**), 197-208.

Veksler, I., Petibon, C., Jenner, G., Dorfman, A. & Dingwell, D. 1998. Trace element partitioning in immiscible silicate–carbonate liquid systems: an initial experimental study using a centrifuge autoclave. *Journal of Petrology*, **39**, 2095-2104.

Verwoerd, W.J. 1993. Update on carbonatites of South Africa and Namibia. *South African Journal of Geology*, **96** (**3**), 75-95.

Wall, F. & Mariano, A.N. 1996. Rare earth minerals in carbonatites: a discussion centred on the Kangankunde Carbonatite, Malawi. *In*: Jones, A.P., Wall, F. & Williams, C.T. (Eds) *Rare Earth Minerals: Chemistry, Origin and Ore Deposits*. Mineralogical Society Series. London, Chapman & Hall, pp. 193-226.

Walter, B.F., Giebel, R.J., Steele-MacInnis, M., Marks, M.A., Kolb, J. & Markl, G. 2021. Fluids associated with carbonatitic magmatism: a critical review and implications for carbonatite magma ascent. *Earth Science Reviews*, article 103509.

Walter, B.F., Steele-MacInnis, M., Giebel, R.J., Marks, M.A.W. & Markl, G. 2020. Complex carbonate-sulfate brines in fluid inclusions from carbonatites: Estimating compositions in the system H_2O-Na-K-CO_3-SO_4-Cl. *Geochimica et Cosmochimica Acta*, **277**, 224-242.

Wei, C. W., Xu, C., Chakhmouradian, A. R., Brenna, M., Kynicky, J. & Song, W.L. 2020. Carbon–strontium isotope decoupling in carbonatites from Caotan (Qinling, China): implications for the origin of calcite carbonatite in orogenic settings. *Journal of Petrology*, **61** (**2**), egaa024.

Weidendorfer, D., Schmidt, M.W. & Mattsson, H.B. 2017. A common origin of carbonatite magmas. *Geology*, **45**, 507-510.

Weng, Q., Yang, W.B., Niu, H.C., Li, N.B., Mitchell, R.H., Zurevinski, S. & Wu, D. 2022. Formation of the Maoniuping giant REE deposit: Constraints from mineralogy and in situ bastnäsite U-Pb geochronology. *American Mineralogist*, **107** (**2**), 282-293.

Woolley, A.R. & Kempe, D.R.C., 1989. Carbonatites: nomenclature, average chemical compositions, and element distribution. *In*: Bell, K. (Ed.) *Carbonatites: Genesis and Evolution*. Unwin Hyman, London, pp. 1-14.

Woolley, A.R. & Kjarsgaard, B.A. 2008. *Carbonatite Occurrences of the World: Map and Database*. Geological Survey of Canada Open File 5796, 28 pp., 1 sheet, 1 CD ROM.

Yaxley, G.M., Anenburg, M., Tappe, S., Decree, S. & Guzmics, T. 2022. Carbonatites: Classification, Sources, Evolution, and Emplacement. *Annual Review of Earth and Planetary Sciences*, **50**.

Zaitsev, A.N., Wall, F. & Le Bas, M.J. 1998. REE-Sr-Ba minerals from the Khibina carbonatites, Kola Peninsula, Russia: their mineralogy, paragenesis and evolution. *Mineralogical Magazine*, **62**, 225-250.

Annex : Major and trace element analyses of samples from Kieshöhe dolomite-carbonatites (DC), calcite-carbonatites (CC), ankerite-carbonatite (AC), diatreme (DI), fenite (F). (X) marks xenolith occurrence. (b.d.l. : below detectable limit; n.a. : not analysed).

Part 1

Sample	KH001	KH002A	KH002A-doublet	KH002B	KH003	KH004	KH005	KH006	KH007	KH009	KH010	KH011	KH012	KH012B	KH013A	KH013B	KH014
Type	*DC (X)*	*DC (X)*	*DC (X)*	*DC (X)*	*DC*	*DC*	*DC*	*DC*	*DC*	*DC (X)*	*CC (X)*	*CC*	*CC(X)*	*CC(X)*	*F (X)*	*CC*	*CC (X)*
SiO_2 (%)	6.68	11.11	11.25	10.90	1.00	0.17	1.40	0.96	0.83	2.03	0.9	1.21	1.80	1.99	74.48	0.66	4.95
TiO_2 (%)	0.04	0.28	0.29	0.24	0.04	0.04	0.05	0.07	0.06	0.04	0.08	0.09	0.08	0.08	0.07	0.17	0.14
Al_2O_3 (%)	b.d.l.	2.75	2.78	2.62	0.22	0.10	0.34	0.13	0.19	0.08	0.17	0.26	0.28	0.17	b.d.l.	0.27	0.21
Fe_2O_3 (%)	8.37	9.69	9.39	8.20	11.5	5.69	11.51	6.57	11.44	8.19	9.43	6.33	4.94	5.98	7.34	6.14	11.16
MnO (%)	5.59	1.44	1.44	1.32	3.63	2.82	3.31	3.47	3.85	3.56	3.26	3.21	2.85	2.95	3.32	2.71	5.67
MgO (%)	11.83	12.60	12.48	11.89	12.59	13.71	11.96	10.47	9.49	13.32	8.86	7.58	7.34	7.83	0.48	5.60	10.99
CaO (%)	20.37	20.85	20.44	20.00	19.71	23.00	21.71	19.76	19.63	21.75	22.43	22.91	21.46	22.30	1.14	39.04	22.53
Na_2O (%)	0.11	0.27	0.26	0.37	0.11	0.10	0.14	0.12	0.14	0.10	0.19	0.17	0.18	0.16	0.04	0.08	0.12
K_2O (%)	0.04	2.19	2.17	1.88	0.09	0.02	0.14	0.01	0.03	0.02	0.03	0.08	0.09	0.03	0.03	0.04	0.07
P_2O_5 (%)	0.10	0.25	0.23	0.18	0.16	0.62	0.13	0.10	0.13	0.08	1.34	0.19	0.19	0.14	0.10	0.61	0.49
Ba (%)	2.17	0.74	0.80	1.88	2.08	1.76	2.50	4.22	3.88	2.33	6.16	7.53	7.05	7.48	3.49	2.26	1.45
Sr (%)	0.35	0.14	0.14	0.18	0.34	0.41	0.19	0.17	0-12	0.21	0.17	0.13	0.16	0.11	0.07	0.45	0.12
LOI	34.23	32.09	32.09	31.54	36.25	39.51	35.50	35.12	32.93	37.27	31.61	34.44	32.31	32.52	4.21	20.47	33.96
Total	98.67	102.53	100.55	99.61	97.22	98.74	98.23	91.01	92.07	99.16	93.72	92.81	89.23	92.81	95..86	83.72	100.65
Trace elements ICPMS in ppm																	
Li	7.38	50.5	n.a.	74.3	7.7	4.2	11.1	15.9	7.3	9.6	5.2	6.5	13.1	4.9	2.9	11.3	4.2
Be	16.5	20.5	n.a	18.2	22.1	9.9	14.9	39.5	35.2	13.3	20.6	15.7	17.8	15.6	15.1	47.1	17.4
Sc	62	59	n.a.	59	71	66	46	48	57	73	47	60	54	70	83	64	101
V	18	126	n.a.	122	74	28	83	131	111	41	46	64	55	43	12	51	60
Cr	9	35	n.a.	33	5	3	7	3	3	4	7	3	3	4	6	4	8
Co	6	18	n.a.	18	22	8	14	10	24	10	5	6	5	3	3	5	4
Ni	8	31	n.a.	33	53	7	25	24	39	33	18	16	13	10	4	10	7
Cu	2	12	n.a.	14	19	3	3	5	4	4	5	5	10	6	3	8	5
Zn	710	312	n.a.	300	1140	1210	1130	850	1680	340	1390	1260	1120	1080	685	990	1240
Rb	0.11	34.7	n.a.	32.5	1.3	0.7	2.8	1.8	2	0.6	0.7	2.4	5	0.5	0.8	1.3	1.4
Sr	3670	1390	n.a.	1880	3820	4450	1940	1870	1070	2250	1570	1110	1630	1030	600	4040	1150
Ba	23000	8000	n.a.	20300	22000	20000	22000	22000	26000	26000	37000	35000	46000	46000	24000	22800	15000
Mo	65	80	n.a.	67	128	43	84	208	137	104	64	60	63	33	112	73	84
Sb	1.6	1.5	n.a.	1.3	0.6	0.3	0.3	0.7	4	0.7	0.5	0.3	0.2	0.2	2.3	1.2	1.1
Cs	0.01	0.6	n.a.	0.6	0.04	0.03	0.09	0.28	0.30	0.02	0.04	0.05	0.21	0.02	0.03	0.05	0.05
Y	154	230	n.a.	200	130	160	170	180	260	180	250	210	230	250	260	340	280
Zr	19	60	n.a.	53	60	4.5	22	105	62	18	18	15	19	19	41	26	25
Nb	20	310	n.a.	217	19	17	42	22	172	280	110	153	80	104	22	100	128
Hf	0.5	2	n.a.	1.5	1	0.4	0.8	1.9	1.5	1.2	0.6	0.9	1.3	1	2.2	0.8	1.4
Ta	0.01	6	n.a.	3.4	0.1	0.1	0.1	0.1	0.1	0.1	0.1	0.1	0.1	0.1	0.1	0.1	0.1
Pb	730	118	n.a.	13	630	990	380	440	1770	410	460	680	300	670	710	890	1200
Bi	1.6	0.7	n.a.	0.7	1.3	3.7	0.7	3.6	5	1.7	6.8	10	2.5	10	3	0.6	1.1
Th	220	170	n.a.	140	310	230	230	100	680	170	240	84	88	87	103	940	248
U	4	8	n.a.	7	7	3	7	10	15	6	9	8	7	8	11	14	8
La	1440	1610	n.a.	1430	1410	1410	1630	5600	2320	1650	620	630	4090	700	900	1940	790
Ce	5910	3270	n.a.	2750	5840	5200	5500	12400	10200	5340	1850	1850	8640	1900	3140	9300	3480
Pr	810	360	n.a.	300	870	720	730	1230	1580	750	300	280	940	260	480	1630	610
Nd	2860	1280	n.a.	1050	3350	2720	2700	3540	6320	2870	1520	1260	3110	1110	2160	7050	2910
Sm	245	140	n.a.	130	330	250	250	240	620	280	350	250	330	200	380	810	520
Eu	45	33	n.a.	31	54	45	47	45	110	51	85	61	76	48	90	140	110
Gd	98	86	n.a.	80	99	89	97	110	220	100	170	130	180	100	200	260	230
Tb	8	11	n.a.	10	7	7	8	9	17	8	17	13	17	12	19	20	21
Dy	33	53	n.a.	45	26	31	34	37	66	35	67	54	66	55	74	77	79
Ho	6	9	n.a.	7	5	5	5	6	9	6	10	8	10	10	11	11	12
Er	14	19	n.a.	17	13	13	12	14	18	13	20	17	19	21	23	23	24
Tm	2	2	n.a.	2	2	2	2	2	2	2	2	2	2	2	2	2	3
Yb	11	12	n.a.	10	14	11	8	11	11	9	10	10	10	11	14	12	13
Lu	1	2	n.a.	1	2	1	1	1	1	1	1	1	1	1	2	1	1
TREE (wt.%)	1.2	0.7	n.a.	0.6	1.2	1.1	1.1	2.3	2.2	1.1	0.5	0.5	1.7	0.5	0.8	2.2	0.9

Part 2

Sample	KH015	KH017	KH018	KH019	KH020	KH021	KH022	KH023A&B	KH023C	KH023D	KH026A&B	KH026D	KH027	KH028	KH029	KH030	KH031
Type	*CC*	*F (X)*	*DC (X)*	*DC (X)*	*DC*	*DC (X)*	*DC*	*DI (X)*	*CC*	*DC*	*DC*	*DC*	*DC*	*DC*	*DI (X)*	*DC (X)*	*DC*
SiO_2 (%)	0.09	57.3	6.47	20.28	1.82	3.89	0.79	88.72	1.00	88.91	1.07	1.04	0.64	0.53	88.47	8.22	1.18
TiO_2 (%)	0.23	1.15	0.13	0.08	0.07	0.07	0.08	0.10	0.02	0.10	0.04	0.04	0.05	0.05	0.08	0.09	0.06
Al_2O_3 (%)	0.17	13.43	1.68	b.d.l.	0.08	0.10	0.22	b.d.l.	0.07	b.d.l.	0.07	b.d.l.	0.13	0.13	0.15	0.15	0.15
Fe_2O_3 (%)	8.32	7.17	4.11	16.07	10.64	8.71	10.15	0.20	3.32	0.18	7.40	7.35	10.29	9.37	1.42	5.08	6.24
MnO (%)	3.44	0.09	0.82	4.59	5.58	3.54	6.5	0.73	1.25	0.73	3.23	3.18	2.53	2.97	0.09	0.75	1.18
MgO (%)	7.92	2.38	12.93	8.9	10.61	12.51	10.04	0.15	10.59	0.15	11.82	11.63	12.02	11.71	1.08	13.52	15.29
CaO (%)	32.97	0.72	24.51	15.83	20.49	20.17	19.31	4.68	24.70	4.67	21.79	21.4	23.73	21.84	3.24	23.67	25.46
Na_2O (%)	0.11	3.57	0.24	0.12	0.16	0.13	0.12	b.d.l.	0.07	b.d.l.	0.14	0.13	0.10	0.13	b.d.l.	0.19	0.08
K_2O (%)	0.01	7.69	1.01	0.04	0.03	0.12	0.03	0.04	0.01	0.04	0.05	0.05	0.04	0.04	0.29	1.71	0.04
P_2O_5 (%)	0.5	0.09	0.10	0.49	0.34	0.4	0.22	0.05	1.95	0.05	0.66	0.66	0.25	0.16	0.21	1.63	0.41
Ba (%)	1.56	0.24	2.70	0.92	2.38	2.57	3.31	0.43	0.59	0.42	2.79	2.76	2.43	2.66	0.29	1.00	0.80
Sr (%)	0.32	0.03	0.25	0.15	0.21	0.17	0.44	0.01	0.49	0.01	0.19	0.19	0.13	0.14	0.02	0.35	0.18
LOI	25.22	4.47	33.04	26.47	33.89	35.29	33.77	4.27	37.96	4.22	36.40	36.84	36.41	36.67	3.92	34.63	41.02
Total	87.51	98.48	97.28	100.50	95.38	97.43	94.18	100.56	92.36	105.31	87.97	95.48	99.07	96.71	100.54	102.31	103.33
Trace elements ICPMS in ppm																	
Li	9	113	93	6	8	20	11	7	23	10	10	7	12	8	10	39	23
Be	34	17	48	49	40	34	61	4	25	24	14	21	18	4	17	35	17
Sc	64	76	118	106	213	101	131	5	35	62	137	26	145	131	23	137	190
V	19	248	51	128	42	27	65	11	43	25	33	113	73	66	157	93	114
Cr	6	33	7	5	9	10	12	3	3	2	2	7	4	7	26	6	16
Co	8	2	3	9	5	9	43	6	4	4	10	16	21	7	11	6	11
Ni	11	17	5	11	13	16	28	9	4	6	14	50	47	18	37	16	18
Cu	3	3	2	1	4	2	5	7	3	6	4	15	5	4	7	0.3	4
Zn	2350	134	396	1060	1790	1300	1090	35	138	1230	1360	1100	1650	85	300	400	200
Rb	0.1	115	25	0.7	0.9	1.1	1.6	0.9	0.7	0.7	0.7	0.1	0.7	4	32	3	15
Sr	2990	271	2500	1470	2200	1630	460	121	5610	5700	1980	1360	1500	221	3550	1900	2770
Ba	16500	2360	29200	9170	26500	26200	25800	4500	6900	15600	30200	25600	29100	3130	11000	8900	7340
Mo	24	23	44	294	213	136	299	37	49	183	94	113	92	20	44	20	10
Sb	2	2	1	5	6	12	14	2	1	3	1	1	1	2	3	1	1
Cs	0.03	2.59	0.57	0.02	0.04	0.03	0.21	0.11	0.16	0.02	0.02	0.04	0.02	0.06	0.35	0.21	0.13
Y	385	46	164	603	1180	1350	1190	40	116	834	494	285	527	540	86	491	1010
Zr	51	450	71	19	27	61	75	17	46	7	26	114	68	34	28	21	143
Nb	189	376	299	56	53	86	69	56	25	12	29	49	34	51	203	349	256
Hf	2	14	2	0.4	2	3	4	0.3	0.6	1.2	0.5	1.7	3.7	0.5	0.8	0.9	1.8
Ta	0.1	0.6	1	0.2	0.3	0.2	0.2	0.1	0.1	0.2	0.1	0.1	0.1	0.3	6	1	8
Pb	1790	17	63	856	1220	900	1020	12	28	1330	1100	525	824	22	73	54	39
Bi	2	0.1	0.3	0.7	0.7	2	0.2	0.1	0.1	7	14	17	23	0.1	0.4	0.1	0.2
Th	747	52	189	510	785	1130	405	7	29	427	345	229	295	77	413	454	153
U	16	6	4	10	8	6	12	2	18	4	6	8	12	5	24	12	16
La	1870	85	2170	1310	8190	5620	3220	51	32700	4950	7720	1040	4340	6880	343	3630	4670
Ce	9813	236	3804	3384	18900	12700	12500	95	50500	15600	19100	6300	9300	15500	617	6470	8530
Pr	1700	34	393	430	2350	1500	1900	11	4510	2870	2240	1240	1130	1870	63	677	928
Nd	7180	160	1270	1660	7700	5020	7260	40	12400	13300	7640	5810	4160	6580	223	2380	3310
Sm	768	32	137	431	920	1140	690	9	649	2520	707	817	520	697	44	606	431
Eu	133	8	34	112	215	293	141	3	100	630	123	153	108	130	14	78	104
Gd	258	19	84	239	504	627	355	11	225	1330	239	278	228	254	39	200	257
Tb	20	2	9	25	51	62	44	2	15	111	19	19	23	22	5	25	33
Dy	80	10	38	116	222	270	230	8	40	359	83	65	108	99	23	1113	186
Ho	12	2	6	20	37	45	41	2	5	41	15	9	19	18	4	19	37
Er	26	4	13	44	83	102	93	3	9	93	40	17	46	47	9	46	97
Tm	2.7	0.4	1.5	5.1	10.3	12.3	10.6	0.4	0.8	5.4	5.3	1.7	5.9	6.0	1.2	6.2	12.4
Yb	13	2	8	26	57	63	52	2	4	24	29	8	31	31	7	35	66
Lu	1.5	0.4	1.0	3.3	7.6	7.8	6.5	0.2	0.6	3.3	3.8	1.1	4.0	4.0	1.0	4.7	8.6
TREE (wt.%)	2.2	0.064	0.8	0.8	3.9	2.8	2.7	0.028	10.1	4.5	3.8	1.6	2.1	3.3	0.1	1.4	2.0

Part 3

Sample	KH032	KHMnSiO4	KH102	KH105A	KH105B	KH107	KH108A	KH108B	KH109	KH110	KH111	KH112	KH113	KH115	KH116	KH117	KH118
Type	*DC (X)*	*DI (X)*	*DI (X)*	*AC (X)*	*AC (X)*	*F*	*DC*	*F*	*F*	*F*	*MC (X)*	*F*	*F*	*AC (X)*	*CC (X)*	*CC*	*CC (X)*
SiO_2 (%)	7.57	39.79	82.06	20.94	25.87	27.36	1.68	30.85	25.89	16.74	17.45	16.75	34.56	0.97	25.56	1.11	0.52
TiO_2 (%)	0.27	0.02	1.12	0.32	0.35	0.77	0.04	0.87	0.96	0.08	0.76	0.95	1.33	0.04	0.67	0.19	0.57
Al_2O_3 (%)	1.42	b.d.l.	0.89	4.79	6.36	4.66	0.42	6.43	5.28	0.26	4.33	3.28	7.27	0.19	4.16	0.12	0.16
Fe_2O_3 (%)	7.29	40.12	8.61	25.83	19.40	13.24	8.73	9.41	17.18	14.95	13.71	15.77	14.84	19.43	4.13	7.73	6.29
MnO (%)	0.48	7.76	0.12	4.24	3.35	2.51	0.85	0.91	1.22	4.55	23.71	3.35	0.48	6.31	0.55	3.38	1.61
MgO (%)	13.95	0.59	0.72	6.25	6.26	6.38	15.33	7.71	7.78	5.37	1.95	7.57	5.27	9.65	9.43	5.54	4.81
CaO (%)	24.46	0.53	0.26	5.88	7.42	12.79	24.74	13.38	12.12	14.83	6.08	16.48	10.86	20.56	19.24	21.22	16.36
Na_2O (%)	0.14	0.03	2.78	0.86	1.25	0.41	0.1	0.71	0.55	0.18	0.42	0.33	0.83	0.05	0.63	0.22	0.11
K_2O (%)	0.95	0.20	0.92	2.82	2.87	3.28	0.18	4.18	3.46	0.11	3.14	2.24	3.94	0.02	1.58	0.01	0.02
P_2O_5 (%)	1.77	0.17	0.04	0.53	1.16	0.51	0.62	0.19	0.32	0.15	0.10	0.57	0.14	0.83	0.17	0.36	0.30
Ba (%)	0.67	0.20	0.45	0.44	0.84	1.00	0.33	0.95	0.52	4.34	4.21	0.66	0.55	1.01	1.08	10.48	3.04
Sr (%)	0.26	0.10	0.01	0.17	0.19	0.08	0.49	0.07	0.06	0.14	0.18	0.14	0.07	0.14	0.26	0.24	0.22
LOI	35.65	8.20	1.55	23.88	22.19	21.75	40.00	20.95	21.60	23.97	14.78	25.74	18.06	32.49	28.24	22.64	45.79
Total	104.45	97.80	99.69	103.61	103.64	99.82	103.95	101.60	101.65	92.19	92.40	100.26	101.95	99.45	102.32	80.88	87.07
Trace elements ICPMS in ppm																	
Li	13	99	32	28	83	12	8	20	11	n.a.	7	50	90	10	42	8	12
Be	51	19	28	30	29	20	40	34	61	n.a.	4	29	19	18	17	27	77
Sc	110	n.a.	264	142	147	118	n.a.	n.a.	n.a.	n.a.		66	82	103	17	53	53
V	110	200	110	95	140	127	42	27	65	n.a.	11	150	210	82	42	56	159
Cr	6	65	63	83	113	30	9	10	12	n.a.	3	115	142	9	21	4	25
Co	20	3	21	16	45	43	5	9	44	n.a.	6	56	13	13	7	7	25
Ni	25	15	107	85	117	82	13	1	28	n.a.	9	180	106	20	11	9	46
Cu	4	6	14	9	38	11	4	2	5	n.a.	7	15	30	1	11	4	23
Zn	1230	101	493	486	1310	850	1790	1300	1090	n.a.	35	890	420	1320	310	1760	2930
Rb	1	7	31	44	34	2	1	1	2	n.a.	1	48	75	1	73	1	3
Sr	3600	71	1580	1940	756	1190	200	1630	4560	n.a.	121	1370	700	1400	2600	1970	6720
Ba	29200	4000	4300	8600	9500	32000	26500	26200	25800	n.a.	4500	6600	5500	10300	11200	56200	84000
Mo	153	36	314	250	140	40	213	136	300	n.a.	37	78	12	252	32	119	245
Sb	17	3	4	3	3	3	6	12	14	n.a.	2	2	2	2	1	1	4
Cs	0.03	0.4	0.7	0.8	0.5	0.3	0.04	0.03	0.21	n.a.	0.11	2.56	3.9	0.03	3.9	0.15	0.23
Y	217	n.a.	131	305	432	670	n.a.	n.a.	n.a.	n.a.	n.a.	274	133	314	74	288	278
Zr	22	520	126	105	147	688	27	61	75	n.a.	17	99	300	12	83	14	50
Nb	7	553	97	90	150	27	53	86	70	n.a.	57	575	180	17	970	78	2280
Hf	0.2	23	4	3	2	7	2	3	4	n.a.	0.3	0.6	7.8	1	31	3	4
Ta	0.2	0.2	0.1	0.1	0.7	0.2	0.3	0.2	0.2	n.a.	0.1	1.7	3.5	0.1	0.7	0.1	1.1
Pb	3080	40	110	94	730	740	1220	900	1020	n.a.	12	465	100	396	660	850	1510
Bi	64	0.3	0.1	0.03	2.1	12	0.7	1.7	0.2	n.a.	0.1	0.8	0.4	0.1	0.2	3.8	0.3
Th	446	59	174	371	560	880	786	1230	405	n.a.	7	222	180	870	240	560	930
U	32	0.3	0.4	0.4	0.6	4.0	17.3	7.8	6.2	n.a.	12.2	2.00	4.3	1.4	13	6.5	13
La	1490	n.a.	51	118	151	1340	n.a.	n.a.	n.a.	n.a.	n.a.	2780	320	340	222	2450	602
Ce	2890	n.a.	184	473	809	5974	n.a.	n.a.	n.a.	n.a.	n.a.	4600	845	3010	908	10800	3150
Pr	307	n.a.	38	98	181	1100	n.a.	n.a.	n.a.	n.a.	n.a.	450	145	733	158	1630	659
Nd	1110	n.a.	215	653	1230	5450	n.a.	n.a.	n.a.	n.a.	n.a.	1490	742	4020	761	6450	3420
Sm	158	n.a.	57	234	400	786	n.a.	n.a.	n.a.	n.a.	n.a.	188	135	520	148	730	600
Eu	42	n.a.	14	54	87	161	n.a.	n.a.	n.a.	n.a.	n.a.	47	31	116	31	137	118
Gd	112	n.a.	34	109	171	334	n.a.	n.a.	n.a.	n.a.	n.a.	118	68	215	58	267	211
Tb	13.6	n.a.	4	11	16	36	n.a.	n.a.	n.a.	n.a.	n.a.	13	8	19	4	19	16
Dy	57	n.a.	22	53	75	160	n.a.	n.a.	n.a.	n.a.	n.a.	61	34	76	17	70	61
Ho	8	n.a.	4	9	13	26	n.a.	n.a.	n.a.	n.a.	n.a.	10	5	11	3	10	9
Er	19	n.a.	11	23	31	56	n.a.	n.a.	n.a.	n.a.	n.a.	22	13	24	6	20	20
Tm	3	n.a.	2	3	4	7	n.a.	n.a.	n.a.	n.a.	n.a.	7	3	2	3	1	2
Yb	17	n.a.	8	20	28	37	n.a.	n.a.	n.a.	n.a.	n.a.	13	9	14	4	13	13
Lu	3	n.a.	1	3	4	5	n.a.	n.a.	n.a.	n.a.	n.a.	2	1	2	1	2	2
TREE (wt.%)	0.6	n.a.	0.08	0.2	0.4	1.6	n.a.	n.a.	n.a.	n.a.	n.a.	1.0	0.2	0.9	0.2	2.3	0.9